Lappeenranta University of Technology
School of Energy Systems
Master`s Degree Programme in Electrical Engineering

Zhuravlev Andrei

EVALUATION OF DIRECT FORCE CONTROL FOR AMB'S ROTOR SYSTEM

Thesis for the degree of the Master of Science (Technology)
Lappeenranta, 2018

Examiners: Professor Olli Pyrhönen
D.Sc. Rafal Jastrzebski
Supervisors: D.Sc. Rafal Jastrzebski

ABSTRACT

Lappeenranta University of Technology

School of Energy Systems

Master`s Degree Programme in Electrical Engineering

Zhuravlev Andrei

Evaluation of direct force control for AMB's rotor system

Master's Thesis, 2018

64 pages, 38 Figures, 2 Tables, 3 appendices

Examiners: Professor Olli Pyrhönen

D.Sc. Rafal Jastrzebski

Keywords: active magnetic bearing (AMB), direct torque control (DTC), direct force control (DFC), electromagnets, current controlled system, flux controlled system, flux estimator.

AMB allows contactless support of a rotating body. AMB requires an active control as it is inherently unstable. Classical current control scheme that consists of outer position and inner current control loops can be used. Another way is to use flux control in the inner loop, in this case flux, estimated from measured currents, is applied. A scheme developed in this thesis is based on DTC principle that is mostly used in electrical drives. This principle is DFC that does not contain inner controller and does not contain current and position stiffnesses that results in faster dynamics. Flux estimator is built for determining force, flux and currents acting in the electromagnets. Controller is LQG with disturbance estimator built for current control, flux control and DFC models. All models are built and compared. Results are analyzed and it can be seen that DFC control has faster dynamics.

ACKNOWLEDGEMENTS

This Master`s thesis was carried out at the Laboratory of Control Engineering and Digital Systems, Department of Electrical Engineering, Lappeenranta University of Technology.

First of all, I wish to express my gratitude to my supervisors D.Sc. Rafal Jastrzebski for regular fruitful meetings, valuable advices and motivation, to Professor Olli Pyrhönen for scientific guidance and support**.** Thanks to "levitated team" for creating inspiring working environment and feeling to be a part of one significant project.

Also I would express my thanks to D.Sc. Katja Hynynen for necessary guidance during all the study at LUT, for friendliness and kindness while answering all disturbing questions.

Last but not least, I am grateful to my mother for encouragement and support throughout all studies.

Zhuravlev Andrei

Lappeenranta University of Technology

November, 2018

TABLE OF CONTENTS

NOMENCLATURE

Symbols

B	magnetic flux density
F_{m}	attractive magnetic force
i_{c}	current
K_{i}	current stiffness
K_{x}	position stiffness coefficient
L	inductance
l_0	nominal air-gap
l_{air}	airgap
m	mass
N	number of coil turns
R	resistance
s	Laplace variable
S_{air}	the smallest cross section area of an electromagnet
t	time
U	voltage
W_{ce}	co-energy
W_{fe}	stored magnetic energy
x	rotor displacement
μ_0	permeability of vacuum
Φ	magnetic flux
χ	force acting angle
ψ	magnetic flux linkage
$\boldsymbol{\Omega}$	rotational speed
ω	angular frequency

Subscripts

A	A end of the rotor with bearing A
air	air
B	B end of the rotor with bearing B
bias	bias
c	control
cl	closed loop
DC	direct current
ff	feed-forward
m	measured
max	maximal
out	output
ref	reference
tri	triangular
x	x axis

LIST OF ABBREVIATIONS AND SYMBOLS

AMB	active magnetic bearing
DC	direct current
DFC	direct force control
DOF	degree of freedom
DSC	direct self-control
DTC	direct torque control
IGBT	insulated-gate bipolar transistor
LQG	linear quadratic Gaussian
Maglev	magnetic levitation
MIMO	multiple input multiple output
MMF	magnetomotive force
PM	permanent magnet
PWM	pulse width modulation
SISO	single input single output

INTRODUCTION

The idea of body levitation in the air has been a dream of humankind since the ancient times. Not far from nowadays the magnetic levitation phenomenon was discovered, and in the 20th century the magnetic suspension principle was for the first time applied in the bearings. Since that time the magnetic suspension of rotors in electrical machines has considerably evolved. The main reasons for the advances in technology are the significant progress in power electronics components and information processing, as well as theoretical development of control systems design.

In this work a novel control principle is presented that does not contain inner controller as well as current and position stiffnesses. It also does not require a flux measurement.

The master's thesis purpose is to design direct force control (DFC) that is based on direct torque control (DTC) principle used in electrical drives, with linear quadratic Gaussian (LQG) position control. Flux and force are calculated via estimator according to measured values of the currents. Control principles are modeled in the software Matlab Simulink. Simulation results of the traditional current controlled system with the bias current, flux controlled system with the bias flux and DFC system are considered and presented.

It is expected that a novel control method will show a better dynamics. We hope to achieve a faster position time response in experimental results.

1 Review of the literature

1.1 Principles of electromagnetic levitation

The idea of using electric and magnetic fields for levitation (or suspension) of bodies has existed for many centuries. Interest in it revived in our century in connection with the development of instrument engineering and engineering for measuring, nuclear, space, cryogenic and other types of modern technology.

It is known that force acts on the electric charge that moves with some speed in an electromagnetic field.

When using permanent magnets, the magnetic force can be either an attractive force or a repulsive force. The strength of the interaction between a ferromagnet and a magnetic field source is always an attractive force. The electrically conductive non-ferromagnetic material and the source of the alternating magnetic field are always repulsed. Two conductors carrying a current can both be attracted and repelled.

The problems of electromagnetic levitation of bodies are devoted to a huge number of works. The first systematic analysis of the possible principles of levitation of bodies using electric and magnetic fields was carried out in 1956 by Boerdijk [1]. In 1964, Geary compiled a fairly complete bibliographic overview of the work of this direction [2].

Electric and magnetic suspensions, depending on the principle of operation, are divided into nine types: electrostatic; on permanent magnets; active magnetic; LC-resonance; induction; conductive; diamagnetic; superconducting; magnetohydrodynamic.

The following sections of this chapter are devoted to a brief presentation of the principles of operation and the main technical characteristics of each of the listed types of suspensions.

1.2 Electrostatic suspension

Idea of electrostatic suspension uses attractive forces between conductive surfaces that have different electrical potentials. One surface belongs to a suspended conductive body, the other surface to a system of electrodes. A vacuum is normally created in the interelectrode space.

To create an uniaxial (single-ended) electrostatic suspension of a charged body, the body is placed in an electric field created by two pairs of electrodes.

Benefits of the electrostatic suspension are the high speed of the control system and the absence of a magnetic field and heat losses. Disadvantages are - the need for high stresses and deep vacuum, low load-carrying capacity. The main application of electrostatic suspension is the suspension of rotors of gyroscopes.

1.3 Suspensions on permanent magnets

Suspensions on permanent magnets (PM) use the magnetic field that is created by permanent magnets or direct current (DC) electromagnets without regulation. The suspended body is partially or completely made of ferromagnetic material and can carry permanent magnets. Suspension of the body (or partial unloading of mechanical supports) is due to magnetic forces of repulsion or attraction. The most used material for the production of permanent magnets is NdFeB (Neodymium Iron Boron).

Particularly it should be noted the fundamental impossibility of implementing a complete non-contact suspension using only permanent magnets. Brownback in 1939 showed that a stable suspension of the body in a constant magnetic field is possible only if the magnetic permeability of the material from which the body is made is less than the magnetic permeability of the environment that is for diamagnetics and superconductors [3].

Due to the noted drawbacks, the permanent magnet supports are mainly used to unload mechanical supports or in combination with active magnetic bearings, as well as in measuring devices.

1.4 Electromagnetic suspension with a resonance circuit

Electromagnetic suspension with a resonant LC circuit (or LC suspension) is one of the simplest and does not require a special suspension regulator. It was first developed in the US by the firm Cambridge Thermionic and is described in the work of Lyman [11].

In the equilibrium position, the forces of attraction of electromagnets are equal to each other. Let the body's balance be broken and it moves a distance to the right. Then the inductance will increase, and decrease. The change in currents and forces will be the opposite: the current and force will decrease, and increase. The resulting attractive force will be directed to the left and the equilibrium position will be restored.

The simplicity of the suspension design is also accompanied by a number of significant drawbacks: low payload; increased energy losses for eddy currents and magnetization reversal; small working clearances. Therefore, the scope of their application is limited to lightly loaded rotors.

1.5 Active magnetic suspension

The sensor measures the displacement of the suspended ferromagnetic body from a given equilibrium position. The measurement signal is processed by the regulator. A power amplifier, powered by an external power source, converts this signal into a control current (in current controlled systems) or into a control flux (in flux controlled systems) in the coil of the electromagnets, which causes the magnetic attraction force in such a way that the disturbed equilibrium position is restored. Also, DFC is considered in this thesis. In such system flux is estimated and force is controlled directly without any current or flux regulating loop. Stability of the suspension, as well as the necessary stiffness and damping, are achieved by the appropriate choice of the control law.

Comparing flux control and DFC some differences can be distinguished, despite of similar operation principle. Both of these systems have force as control signal. Flux control has a linear regulator in the inner control loop and typically a voltage PWM, while DFC does not have the inner control loop but the modulator for every electromagnet. These modulators find necessary voltage for electromagnets depending on the reference force. Absence of inner control loop in DFC makes it possible to achieve a faster position response while using suitable tables reducing modulation delay.

In general, active magnetic suspension in comparison with the suspension on permanent magnets has the following main advantages: the carrying capacity is much higher; high mechanical strength; the possibility of implementing a stable non-contact body suspension; the possibility of varying the stiffness and damping within a wide range. The drawbacks of an active magnetic suspension include: the presence of an external power source and the relatively higher complexity and cost caused by the presence of an electronic control

unit. Due to its undeniable advantages, it is the type of suspension that is most widely used in engineering.

1.6 Induction suspension

The principle of the induction suspension is based on the fact that the suspended electrically conductive body is placed in the high-frequency alternating magnetic field of the electromagnet, and the suspension is carried out due to repulsive forces of the main field and the eddy currents induced by this field in the suspended body. It is also possible the reverse option of induction suspension, when the electromagnet powered by a high-frequency voltage soars above the electrically conductive surface.

It should be noted that if the suspended body has a large magnetic permeability, then in addition to the repulsive force of induction, there is a significant force that attracts the body to the electromagnet. Therefore, the use of induction suspension for suspending ferromagnetic bodies is inexpedient.

The review of the induction suspension is carried out by A.A Fomin [12] - [7]. Important field of application of this suspension type is the crucibleless melting of ultrapure metals. Its main idea is that a piece of metal is induction heated and melted by the energy of the magnetic field of the suspension.

A variety of induction suspension, consisting of a stationary electrically conductive rail and a permanent superconductor magnet mounted on a moving vehicle, is used in the development of high-speed ground transport on a magnetic cushion.

Simplicity of construction, ability to work in aggressive environments and vacuum, as well as at high speeds, the possibility of creating frictionless supports are properties that allow to use the induction suspension in devices for various purposes, from equipment of accurate physical experiment to power

engineering and transport. A significant drawback of large energy costs (up to 100W per 1N load) is the main obstacle to the widespread practical implementation of induction suspension.

1.7 Conductive, diamagnetic and superconducting suspensions

The principle of the conductive suspension is based on the displacement of the conductor with current from the magnetic field. According to the current type conductive suspensions are divided into DC suspensions and AC suspensions (the magnetic field and current must coincide in phase). As well as induction suspensions, conductive suspensions are most often used for crucibleless melting of ultrapure metals but can also be used in transport devices.
The main drawback is the need for a large current source, which requires the presence of a contact or non-contact device for power transmission.
The principle of the action of the diamagnetic suspension is based on the fact that a diamagnetic placed in a magnetic field is magnetized in the direction opposite to the direction of the field and is pushed out of the magnetic field. The best diamagnetics are graphite and bismuth. Load capacity of diamagnetic suspension is extremely small. Areas of possible application are kinematic sensors and sensors for measuring instantaneous forces.
Superconducting suspension includes a superconductor mounted on a suspended body and a conventional or superconducting electromagnet. The principle of their action is based on the fact that the magnetic field does not penetrate into the body of the superconductor and it is thus an ideal diamagnetic that is repelled by the magnetic field. This circumstance removes the "Irnoshow prohibition" and allows creating a suspension of a superconducting body without an external stabilization system.

1.8 Magnetohydrodynamic suspension

The development of nuclear and magnetohydrodynamic power engineering and metallurgy led to the creation of pumps, metering devices and other machines working with liquid metals and ionized gases at temperatures up to 12000C (sodium, potassium, lithium, and so on). The use of conventional bearings here is accompanied by considerable difficulties. The logical solution is to use as a lubricant the working agent itself that is liquid metal or gas. However, the latter have low viscosity, and the lubricating layer formed by them is of low lifting capacity. The imposition of magnetic fields on the lubricating layer, as well as the passage of electric current through it, can significantly increase the load-bearing capacity of such supports, called magnetohydrodynamic bearings.

Comparing the advantages and disadvantages of the various types of electromagnetic suspensions considered above, it can be concluded that the most practical interest in terms of wide industrial use in the bearing assemblies of rotary machines is the active magnetic suspension. Bearings operating on the principle of active magnetic suspension and commonly referred to as AMB, and will be the subject of further consideration.

Magnetic levitation systems with different operating principles are compared in [8] and [11].

2 General control principles and plant implementation

2.1 Characteristics of active magnetic suspension

In an AMB magnetic force allows to support a rotor in an electrical machine without any physical contact. This feature allows to eliminate the important issue of drive maintenance – bearing lubrication and renewal [10]. Due to the absence of lubrication oil motor drives designed on the magnetic levitation principle can be used in applications where conventional bearings can not provide the desired features. Among the other important benefits of AMBs the following can be stated:

• High rotational rotor speed that is limited only by the rotor material strength.

• Active rotor dynamics control through the bearings [2].

• AMBs ensure high vibration insulation and lower power losses in comparison with the fluid film bearings [3].

In accordance with the mentioned benefits the list of possible applications is as follows:

• medical and pharmacy equipment;

• outer space equipment;

• equipment exploited in severe environments and undergoing radiation and poisonous substances;

• electrical drives operating in vacuum without contamination;

• MAGLEV trains;

• precise machine tools [8].

However, several drawbacks are mentioned in [11].

• Load capacity failure due to a breakdown of any single component.

• Maintenance operations are impossible without qualified personnel.

• In general, higher costs, weight and space requirements in comparison with conventional bearings.

2.2 Structure of 1 DOF AMB system

AMB is a clear example of a mechatronic product, as the hardware part of a system with AMBs comprises mechanical components aggregated with electronic elements and information processing unit. Software of an AMB system is another crucial part, and the designed control models define the further system efficiency. In a typical mechatronic system forces and motions are produced in accordance with the input signals processed by the system.

AMB system consists of following main parts: AMBs, control unit, auxiliary bearings, position sensors and power electronics.

The simple structure of 1- degree of freedom (DOF) magnetic levitation system is presented in Figure 2.1. The radial displacement along x-axis is detected by the displacement sensor. Outer position controller is fed with the feedback signal coming from the position sensor, and provides the control signal to control system. Depending on type of control system used, different control laws are applied but all of them provide necessary modulated voltage as an output that is finally fed to the electromagnet, current or flux feedback are used in the inner control loop. The control law determines the levitation stability and both stiffness and damping of a magnetic suspension. A series-wound coil around the electromagnet is excited by the provided voltage. Electromagnetic flux Φ changes that results in the magnetic attractive forces change. The flux path is represented by dashed line.

To provide the rotor levitation, generated magnetic attractive force must be sufficient to compensate gravity. Thus, the generated attractive force should be in the opposite direction of the gravity force:

$$F_{\mathrm{m}} = -F_{\mathrm{g}} = -\left(-mg\right) = mg\,, \tag{2.1}$$

where F_{m}, F_{g}, g are attractive magnetic force, gravity force and gravity acceleration, respectively.

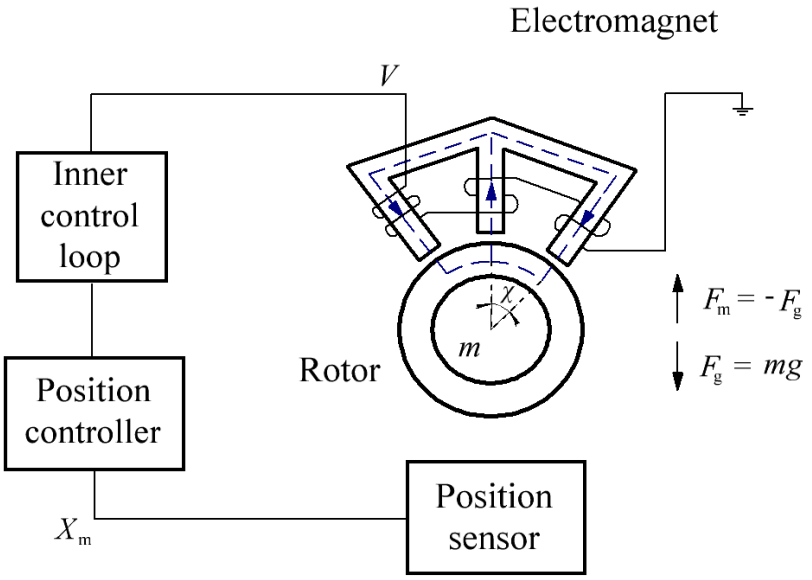

Figure 2.1 – 1 DOF magnetic levitation system [10]

Rotor now is simply a point mass. The radial displacement is obtained as a double integration of acceleration:

$$x = \iint a\,, \tag{2.2}$$

where x is the radial displacement and a is acceleration of the rotor.

The system transfer function for point mass rotor can be expressed as:

$$G\left(s\right) = \frac{K_{\mathrm{i}}}{ms^2 - K_{\mathrm{x}}}\,, \tag{2.3}$$

where K_{i} and K_{x} are current and position stiffnesses, accordingly; m is mass and s is the Laplace operator.

Transfer function poles:

$$s = \pm\sqrt{\frac{K_{\mathrm{x}}}{m}}\,. \tag{2.4}$$

One of the poles is located in the right half plane, thus a negative feedback is necessary for stable operation.

Position stiffness K_x and current stiffness K_i are used in controller for current controlled system. These coefficients linearized about the operating point are considered in the next subchapter.

2.3 Actuator model

Magnetization of electromagnets can be analyzed using simplified equivalent magnetic circuit shown in Figure 2.2. Leakage fluxes and end effects are neglected.

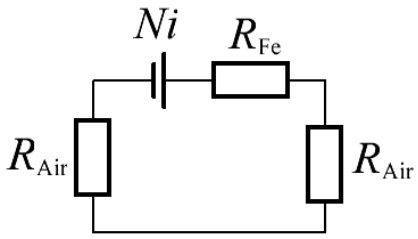

Figure 2.2 – Equivalent magnetic circuit of electromagnet

The voltage source Ni represents the magnetomotive force (MMF) generated by current in the winding. R_{Fe} and R_{Air} represent magnetic resistance of the iron path and magnetic resistance of the air gap, respectively. The magnetic circuit Equations are:

$$l_{\text{Fe}}H_{\text{Fe}} + 2l_{\text{Air}}H_{\text{Air}} = Ni\,, \tag{2.5}$$

where l_{Fe} and l_{Air} are flux paths in the air and iron, accordingly; H_{Fe} and H_{Air} are magnetic field strengths in the air and iron, accordingly; N is number of coil turns and i is current in the coil wire.

Taking into account Equation for magnetic field strength through flux density:

$$H = \frac{B}{\mu_0\mu_{\text{Fe}}}, \tag{2.6}$$

where μ_0 and μ_{Fe} are permeabilities of vacuum and iron, accordingly.

And Equation for flux density through flux:

$$B = \frac{\Phi}{S}, \tag{2.7}$$

where Φ and S are flux and cross section area of electromagnet, accordingly.

Magnetic circuit Equation through flux is obtained:

$$l_{Fe}\frac{\Phi}{\mu_0\mu_{Fe}S} + 2l_{Air}\frac{\Phi}{\mu_0 S} = Ni\,. \tag{2.8}$$

Presented plant model for 2 opposite electromagnets is flux based. It takes into account iron saturation and inductance changes depending on the position of the rotor. Building a plant model requires both Ohm's Law for magnetic circuit and Ohm's Law for the electric circuit running in parallel.

Taking into account that flux linkage is a total flux in N coil turns:

$$\Psi = \Phi N\,, \tag{2.9}$$

where Ψ is flux linkage.

Based on Equations 2.6 and 2.7 Ohm's Law for magnetic circuit presents flux linkage, depending on displacement, in the electromagnet according to the following Equation:

$$\Psi = \frac{\mu_0 NiS}{2\left(l_0 \pm x\right) + \frac{l_{Fe}}{\mu_{Fe}\left(\Phi\right)}}, \tag{2.10}$$

where l_0 is nominal airgap length; "+" sign is used for determining position displacement in the lower electromagnet and "-" in the upper one, respectively; permeability of iron μ_{Fe} (Φ) is obtained from $B(H)$ curve for the used steel type that is "Sura NO 20" and implemented as a look-up table-based magnetic saturation model.

Ohm's Law for the electric circuit presents voltage according to the following Equation:

$$u = Ri + \frac{d\Psi}{dt}. \tag{2.11}$$

where u is voltage and R is resistance.

On the other hand, flux is the function of two independent variables. According to the differentiation rule for complex functions, we have:

$$\frac{d\Psi}{dt} = \frac{\partial \Psi}{\partial i}\frac{di}{dt} + \frac{\partial \Psi}{\partial x}\frac{dx}{dt}. \tag{2.12}$$

As a result of taking the derivative and substituting it in Equation 2.11, voltage for upper and lower electromagnets can be expressed as follows:

$$u = Ri + \frac{\mu_0 N^2 S}{2\left(l_0 \mp x\right) + \frac{l_{\mathrm{Fe}}}{\mu_{\mathrm{Fe}}\left(\Phi\right)}} \cdot \dot{i} \pm \frac{1}{2} \cdot \frac{\mu_0 N^2 i S}{\left(2\left(l_0 \mp x\right) + \frac{l_{\mathrm{Fe}}}{\mu_{\mathrm{Fe}}\left(\Phi\right)}\right)^2} \cdot \dot{x}, \tag{2.13}$$

where current stiffness is equal to:

$$K_{\mathrm{ii}} = \frac{\mu_0 N^2 i S}{\left(2\left(l_0 \mp x\right) + \frac{l_{\mathrm{Fe}}}{\mu_{\mathrm{Fe}}\left(\Phi\right)}\right)^2}, \tag{2.14}$$

and inductance that includes saturation and depends on position displacement is equal to:

$$L = \frac{\mu_0 N^2 S}{2\left(l_0 \mp x\right) + \frac{l_{\mathrm{Fe}}}{\mu_{\mathrm{Fe}}\left(\Phi\right)}}. \tag{2.15}$$

Current stiffness linearized about operating point can be expressed as:

$$K_{\mathrm{i}} = \frac{\mu_0 N^2 i_{\mathrm{bias}} S}{l_0^{\,2}}, \tag{2.16}$$

where i_{bias} is biasing current.

Position stiffness is equal to [11]:

$$K_{\mathrm{x}} = \frac{\mu_0 N^2 {i_{\mathrm{bias}}}^2 S}{l_0^{\,3}}. \tag{2.17}$$

Force in the electromagnet depends on the flux according to the Equation [12]:

$$f_{up} = \frac{\Phi_{up}{}^2 cos\chi}{\mu_0 S}, \tag{2.18}$$

where f_{up} is force in upper electromagnet and $cos\chi$ is force acting angle.

Figure 2.3 illustrates nonlinear flux based model of the upper electromagnet that is built by derived Equations.

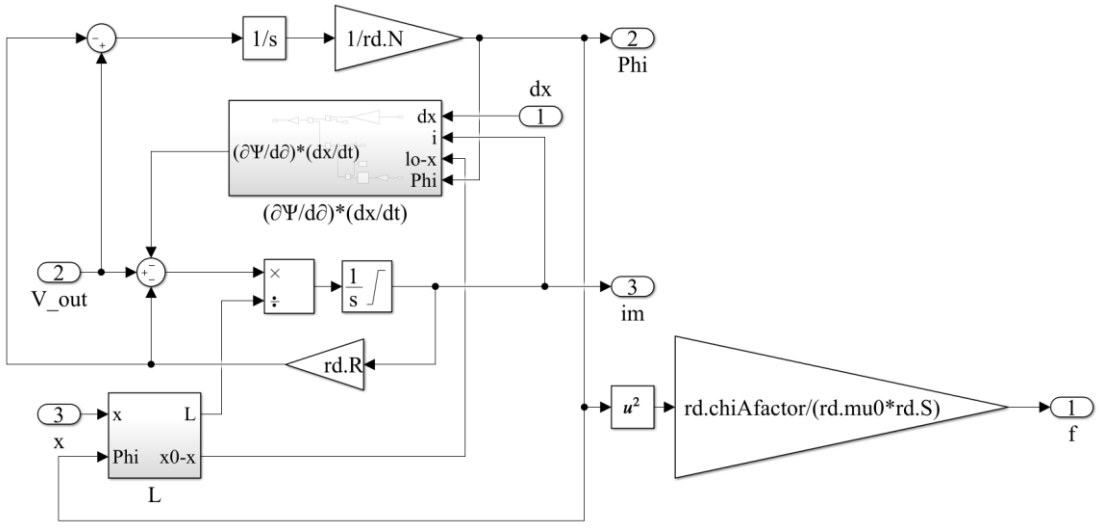

Figure 2.3 – Flux based model of the upper electromagnet built on full equation

The rotor radial force generation principle in AMB is illustrated in Figure 2.4. Stator core surrounds a rotating shaft. In full AMB model strong magnetic attractive forces are generated by eight magnetic poles in N, S, N, S sequence between the rotor and stator cores as illustrated below, although for simplicity plant model consists only of two, upper and lower electromagnets.

In Figure 2.4 the right electromagnet has stronger flux density than the remaining ones that results in the rotor radial force generation in the direction represented by the black arrow.

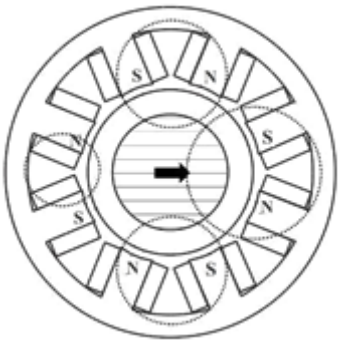

Figure 2.4 – Radial force generation by unbalanced airgap flux density [10]

Resulting force of action of both electromagnets is equal to the difference of produced forces:

$$f = \frac{\cos\chi}{\mu_0 S}(\Phi_{up}{}^2 - \Phi_{low}{}^2). \tag{2.19}$$

Plant model for the system with point mass rotor and two electromagnets looks in the following way:

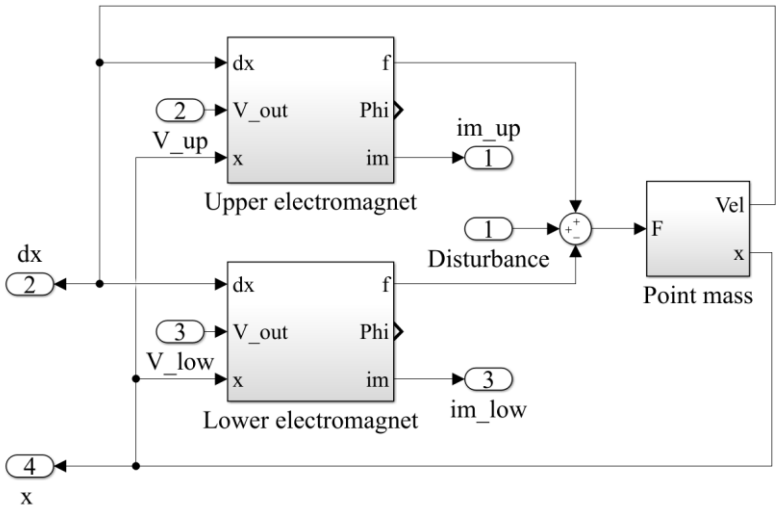

Figure 2.5 – Plant model with point mass rotor and two electromagnets

This plant model is used for simulation in all 3 systems: current control, flux control and DFC. All control principles are considered in more detail in up-coming chapters.

2.4 4 DOF rigid rotor model

More accurate information about processes acting in the real AMB rotor system can be obtained using a more complex rotor model such as rigid rotor. Rigid rotor control system currently is under developing and is mentioned here only for information purposes. It might work with retuned single input single output (SISO) controller but in most cases it requires a multiple input multiple output (MIMO) controller to be applied. Process of deriving matrices for the rotor is shown in Appendix 3.

To obtain practical numerical results it is necessary to extend rotor model to 4-DOF system, so brief review is required. Generally, in 4-DOF system the rotor is levitated by two radial bearings and one axial bearing. Radial bearings provide the generation of magnetic forces in two dimensions along x and y axes; axial bearing generates force along z axis. Auxiliary bearings are used to prevent a rotor touchdown under the condition of high shock load or other failures in the bearing winding or other circuitry. The electromagnetic levitation principle for the 4-DOF magnetic bearing system is shown in Figure 2.6.

In AMB system rotor is a complicated device consisting of several components. Rotor is a solid steel shaft with a stack of circular laminations fitted to the shaft at the area of radial AMBs installation. The laminations are used to prevent high eddy current losses and to ensure high magnetic permeability. A rotor also includes a solid steel disk used for the axial AMB.

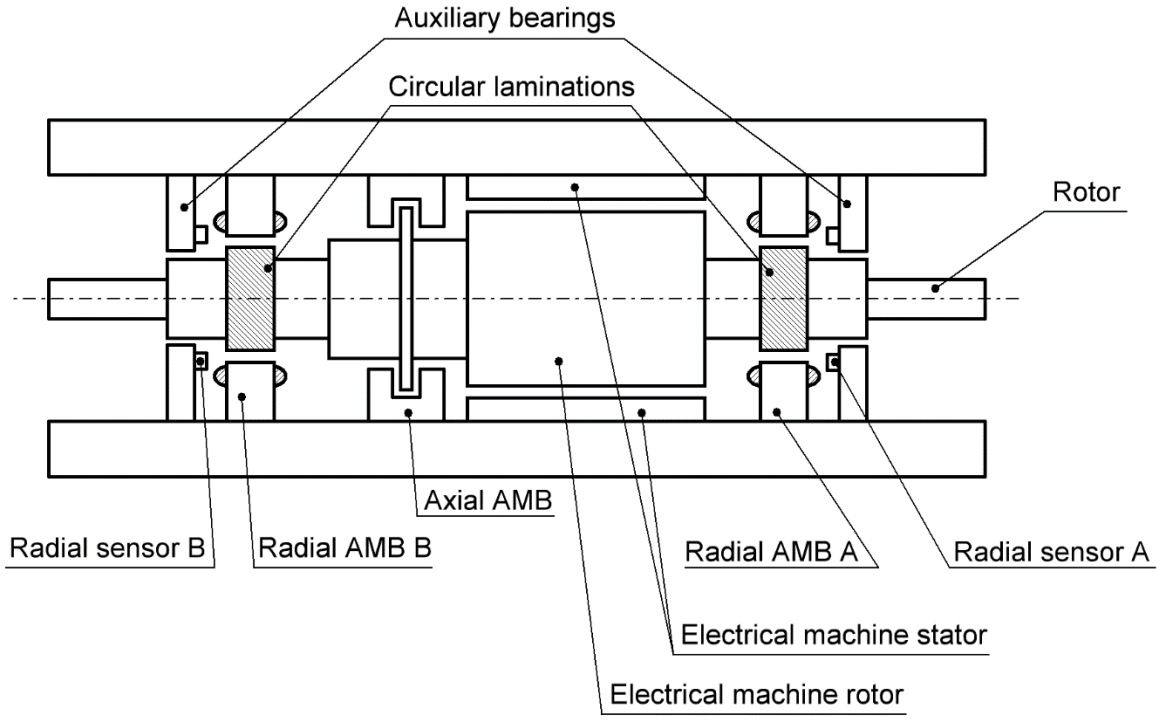

Figure 2.6 –AMB system with 4 degrees of freedom [10]

The axial AMB stator is used for a double-acting thrust bearing installation [11].

The operating position range that is lately referred to as (x_{min}, x_{max}) and (y_{min}, y_{max}), is determined by the airgap length between the auxiliary bearings and the rotor.

Final aim of providing research is to develop a new control system. To estimate reliability of results achieved it is necessarily to obtain numerical results while applying the control model to a prototype. Numerical results from the prototype have not been obtained in this work, and only simulation results from software Matlab Simulink are presented. However, numerical results are going to be provided in further paper. Accurate parameters of the prototype as a controlled object are shown in Table 2.1.

Table 2.1 – Parameters of the test rig

Parameters	**Values**	**Units**
Rotor mass	19.2230	kg
Number of coil turns	260	
Nominal inductance	0.0323	H
Nominal resistance	0.5911	Ω
Nominal airgap	0.0008	m
The flux path in the iron	0.108	m
Mechanical airgap	0.0004	m
Biasing current	2	A
Saturation current	5.8765	A
DC link voltage	150	V
Permeability of vacuum	$4\pi \cdot 10^{-7}$	H/m
Cross section area of an electro-magnet	$6.0850 \cdot 10^{-4}$	m2
Force acting angle, ($\cos\chi$)	0.9724	
Position stiffness	$3.9269 \cdot 10^{5}$	
Current stiffness	157.0768	
Max force	923.0620	N
Force bias	9.2306	N
Flux bias	$8.5198 \cdot 10^{5}$	Wb
Sample time	100	μs
Min possible switching time	4	μs

Schematic blueprint with sizes of the test rig rotor, to which developed systems is going to be applied is shown in Figure 2.7.

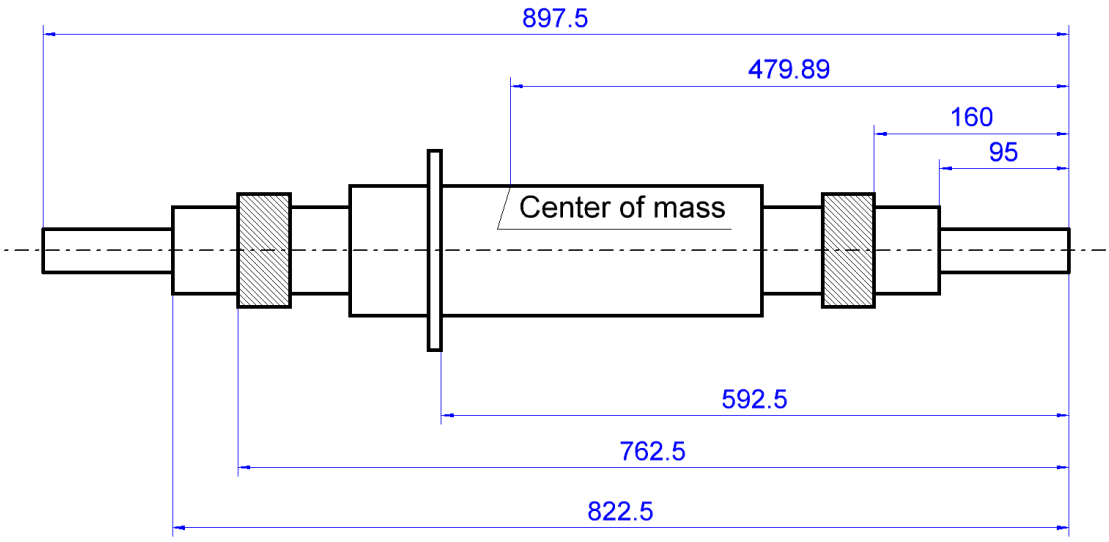

Figure 2.7 – Schematic blueprint with sizes of the test rig rotor

Presented blueprint is used for developing a more complex rotor model such as rigid rotor, and also the flexible rotor that takes into account band modes in further work. It is not used in current research and it is presented only for informational purposes.

The rotor position should be kept in the operating position range. For the rotor displacement evaluation purpose position sensors are used. Among the specific requirements to the position sensors are the following features: the sensors should be contactless, have decent linearity and sensitivity in the measurement range, as well as low noise susceptibility. Sensor type that is used in the prototype is described in [11].

2.5 Overall plant model

Overall plant model is built on following equations.

$$x = \iint \frac{f_{res}}{m}, \tag{2.20}$$

where f_{res} is resulting force of acting both upper and lower electromagnets.

$$f_{res} = f_{up} - f_{low} + f_{dist}, \tag{2.21}$$

where f_{dist} is disturbance force.

$$f_{up(low)} = \frac{\Phi_{up(low)}{}^2 cos\chi}{\mu_0 S}; \tag{2.22}$$

$$u = Ri + \frac{\mu_0 N^2 S}{2(l_0 \mp x) + \frac{l_{Fe}}{\mu_{Fe}(\Phi)}} \cdot \dot{i} \pm \frac{1}{2} \cdot \frac{\mu_0 N^2 i S}{\left(2(l_0 \mp x) + \frac{l_{Fe}}{\mu_{Fe}(\Phi)}\right)^2} \cdot \dot{x}. \tag{2.23}$$

Different control principles are considered in next chapters.

3 Current control system

3.1 Outer position control loop

The block diagram of a control system with two loops that are inner current control loop and outer position control loop are shown in Figure 3.1. Position controller in all developed models is implemented based on LQG. Structure of the outer position control loop is same for all systems. Electromagnet model used is nonlinear, as there are quadratic dependences, current and voltage amplifier limits; force and the inductance depend on the displacement of the rotor.

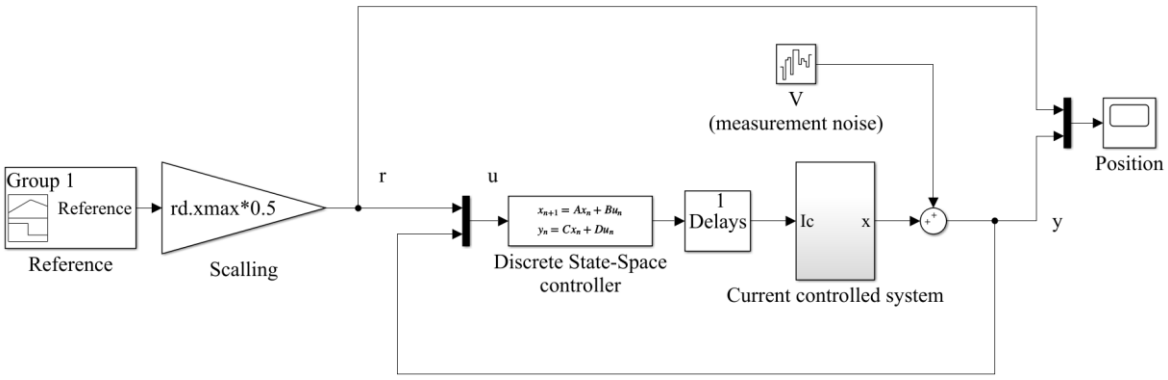

Figure 3.1 – Outer position control loop for current controlled system

Tuning of the linear quadratic regulator is based on the theory of linear matrix inequalities. The controller includes disturbance observer. It is assumed that the disturbance is not measured and it is an external parasitic influence of a controlled object. We consider a LQ law governing the control of a discrete object in the case of a measurable state. Such a control law ensures the asymptotic stability of a closed system, and the LQ minimizes the quadratic functional in the case of a given initial state of the object.

All physical parameters are defined in M-Files, part of which can be found in Appendix 1. The state-space model is created in the physical and per unit systems. Both systems represent the same model, as the eigenvalues are equal. System is augmented for disturbance estimation. Controller gain is obtained using LQG, function *K = lqr()*, augmented system is not used because augmented one is always not controllable. Estimator gain is obtained using pole-placement. Natural frequency, ω_n, damping ratio, ζ, and integral gain, α, are varied to get desired poles. Function *L = acker()* is used to obtain estimator gain. Then state-space model for closed loop with disturbances and noise including controller and disturbance estimator is derived. State-space model for controller is obtained and then sensitivity is calculated. The poles are adjusted (by changing ω_n, ζ and α) to get suitable sensitivity (S_o <3).

Output sensitivity is calculated in the following way:

$$S_0 = \frac{1}{1 - Gc} \cdot sysC, \tag{3.1}$$

where G_c is the model of the regulator; *sysC* is model plant.

Zeros and poles of the output sensitivity and closed loop transfer function are equal, so sensitivity is found correctly.

Input sensitivity from control effort to disturbance is equal to output sensitivity that is suitable for SISO but may not be valid for MIMO system.

Q and *R* matrices are selected to get a trade-off between performance and value of the sensitivity function, which in accordance to the standards for the magnetic, suspensions must be less than 3 (*S* <3).

Controller for the used model is tuned in the following way.

$$R = 0.1\left[\frac{1}{i_{\max}^{\ 2}}\right]; \tag{3.2}$$

$$Q = 0.1\begin{pmatrix} \dfrac{1}{(5x_{\max})^2} & 0 \\ 0 & \dfrac{1}{(20000V_{\max})^2} \end{pmatrix}. \qquad (3.3)$$

While disturbance observer is tuned in the following way.

$\omega_n = 4000\,rad/s$;

$\zeta = 0.5$;

$\alpha = 0.25$.

Open loop poles are shown in Figure 3.2.

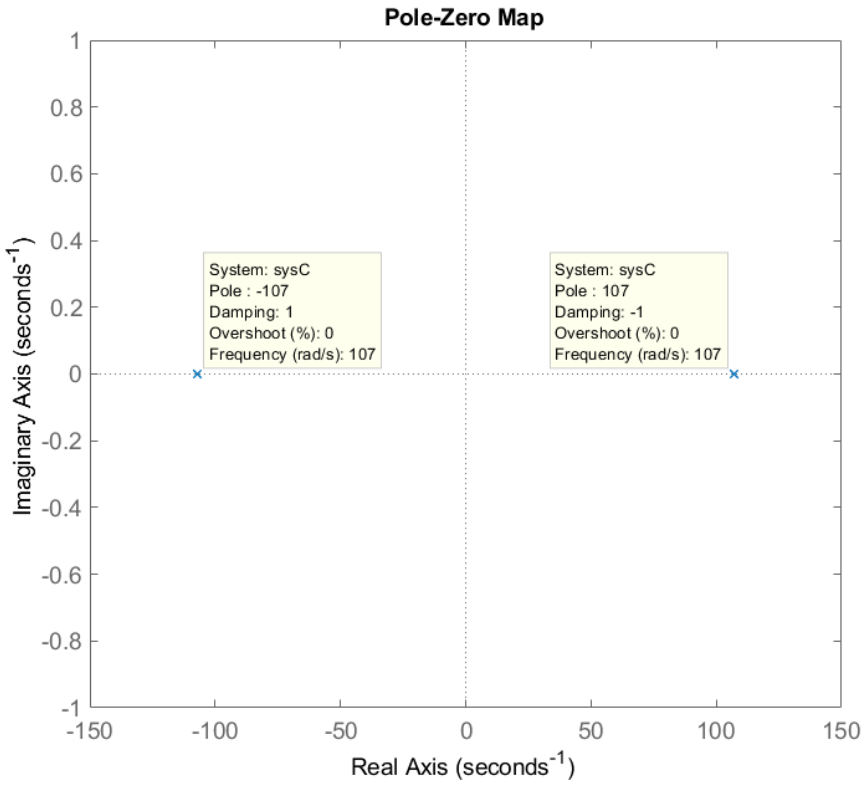

Figure 3.2 – Open loop poles

Current controlled model is discussed in more detail in the next section.

3.2 Inner current controlled loop

Current controlled model comprises current biasing block, block that contains the current control loop for each electromagnet, a non-linear model for each of the electromagnets and the rotor model as a point mass. In the following work, the rotor is going to be extended to a system with 4 degrees of freedom. Current controlled model is shown in Figure 3.3.

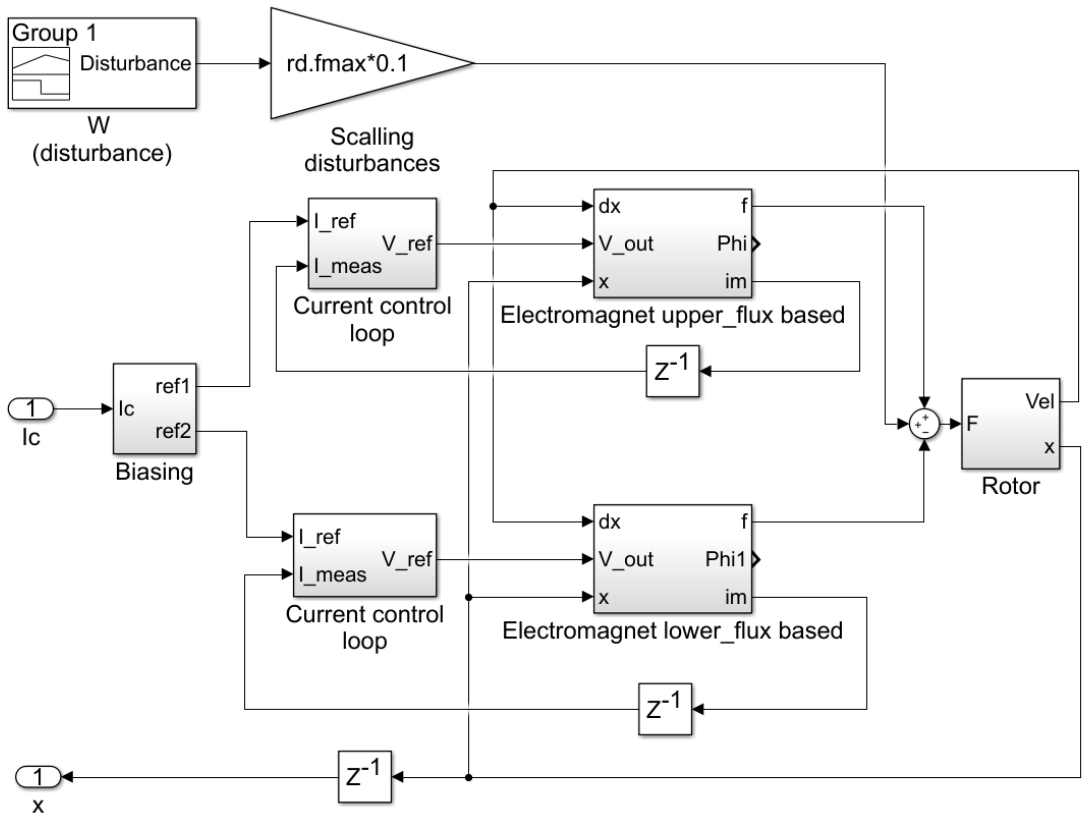

Figure 3.3 – Current control system

Current biasing block provides two reference signals: for upper and lower electromagnet as shown in Figure 3.4.

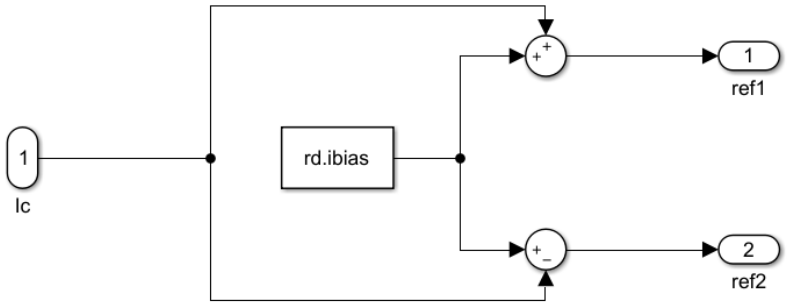

Figure 3.4 – Current biasing block

Block that contains the current control loop is shown in Figure 3.5.

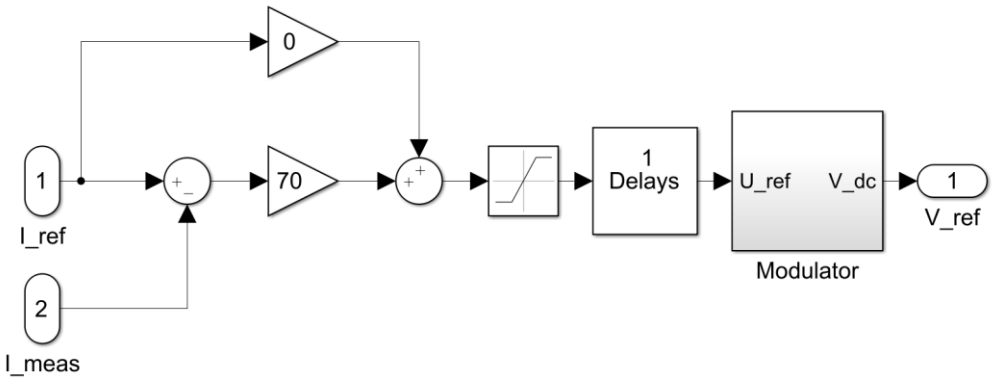

Figure 3.5 – Inner current control loop

Current control is based on feedback of measured value of electromagnet current, which reduces the influence of the nonlinear behavior of the inductance. The feedforward gain is used to compensate for the voltage drop, and correct errors in the steady state caused by pulse width modulation (PWM).

Neglecting the coil resistance, assuming no voltage saturation and no modulation PWM or measurement delays, and assuming nominal inductance, the closed inner-loop current control dynamics, G_{cl}, can be approximated in the s-domain by [12]:

$$G_{\mathrm{cl}} = \frac{i_{\mathrm{m}}}{i_{\mathrm{r}}} \approx \frac{K_{\mathrm{c}}}{Ls + K_{\mathrm{c}}}. \tag{3.4}$$

where i_m is the measured current. The loop bandwidth is approximately equal to the current feedback gain, K_c, divided by the nominal inductance, L. For such an approximation, the rise time is inversely proportional to the bandwidth $\omega_{bw} = \frac{\ln(9)}{t_{rise}}$. Assuming the rise time from 10% to 90% of the steady-state maximum current value, i_{max}, the K_c can be roughly selected, so as to ensure no voltage saturation:

$$K_c < \frac{ln(9)L}{t_{rise}} \approx \frac{ln(9)u_{dc}}{0.8i_{max}} = 70\,. \qquad (3.5)$$

The developed method of current control can be considered as a first order process with a time delay. According to the study of D.M. Schneider, processes with large time constants are difficult to control, and thus, the inner current control loop should be stable and provide a low sensitivity to changes of the parameters [13].

The nonlinear model of the electromagnet has been described above, modulator that simulates switching of half-bridge insulated-gate bipolar transistors (IGBT) circuit is added to the system [7].

3.3 Power electronics and modulator

Coil current is generated using a three-phase linear diode rectifier and a power amplifier. Power amplifier is a half-bridge switching amplifier consisting of two diodes and two IGBT-switches. The switching circuit is created using PWM. Each IGBT-switch has its own control voltage $\pm u_c$, which is compared with a reference signal u_{tri}. As a result, the output voltage varies from zero to $\pm U_{dc}$ (intermediate circuit voltage) in accordance with the IGBT configuration [8]. The power circuit is shown in Figure 3.6.

The modulator includes a control system using PWM and a half-bridge circuit.

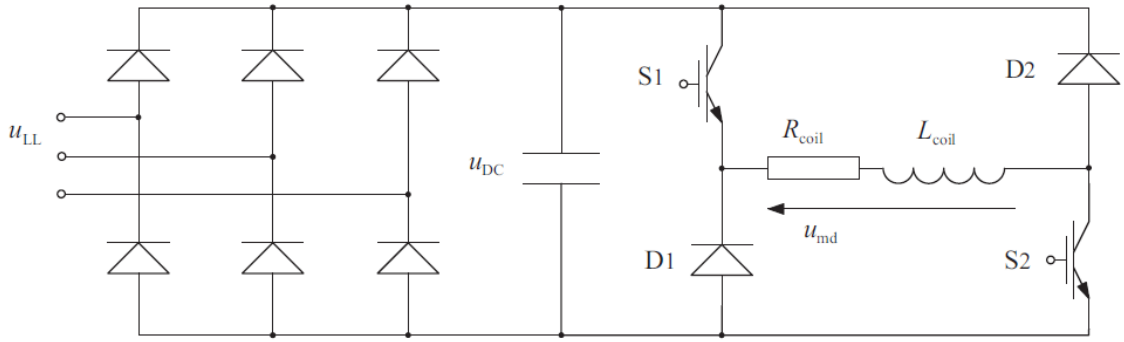

Figure 3.6 – A half-bridge circuit with two switches [11]

PWM provides 3 voltage levels: -150, 0 and 150 V.

When $u_{ref} > u_{tri}$, S1 switch is turned on.

When $u_{ref} > -u_{tri}$, S2 switch is turned on.

This scheme is modeled in following way as shown in Figure 3.7.

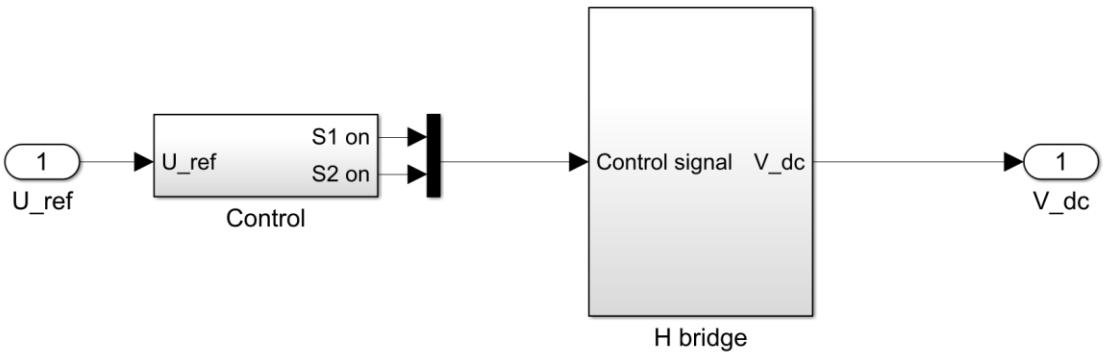

Figure 3.7 – Modulator simulating switching of half-bridge circuit IGBTs

«Control» block generates switch control pulses for a half-bridge circuit according to the logic presented above. Modulator receives a desired voltage value at the input, and provides modulated signal at the output. The resulting voltage is supplied to the electromagnets, each electromagnet has a half-bridge circuit with its control unit.

«Control» block modeled as shown in Figure 3.8.

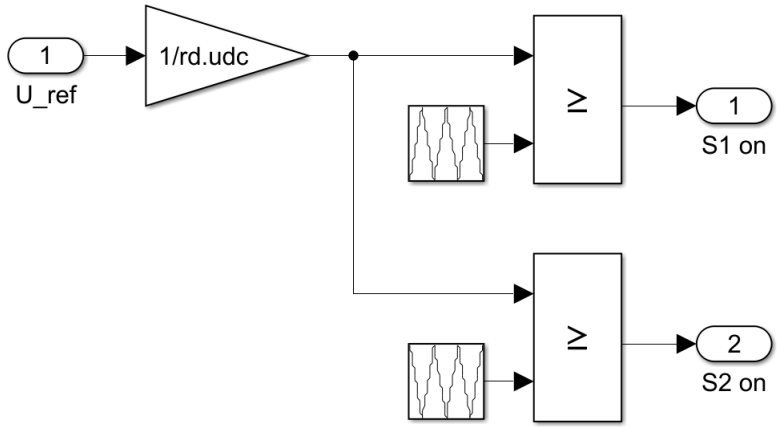

Figure 3.8 – «Control» block

A desired voltage signal is compared with two triangular signals, where the first one is in opposite phase to the second one. As a result, control signals for the upper «S1 on» and lower «S2 on» switches are obtained in this block.

A half-bridge circuit block «H bridge» is modeled as shown in Figure 3.9.

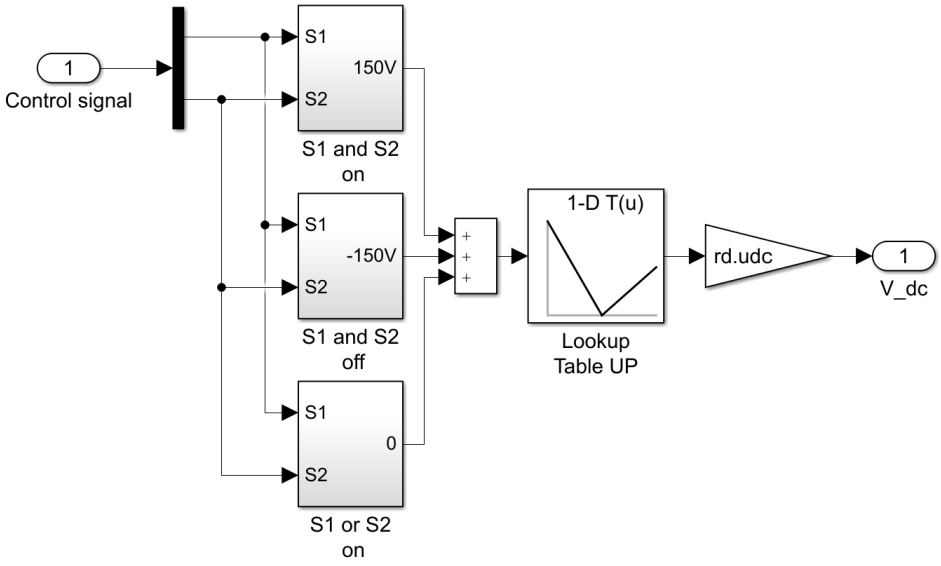

Figure 3.9 – «H bridge» block

3 voltage levels are generated depending on the control signals supplied to the half-bridge circuit switches.

Circuit provides voltage 150V at the time moment when signals are applied to the both switches (block «S1 and S2 on»).

At the time moment when both control signals are zero, the output voltage of -150V is generated (block «S1 and S2 off»).

If control signal is applied to only one switch, so second one is fed by zero, the circuit provides a zero voltage (block «S1 or S2 on»).

3.4 Simulation results

A complete state-space model with disturbances and noise is created. We get frequency response (Bode plot), to determine the sensitivity function to disturbance and noise. The graph is shown in Figure 3.10.

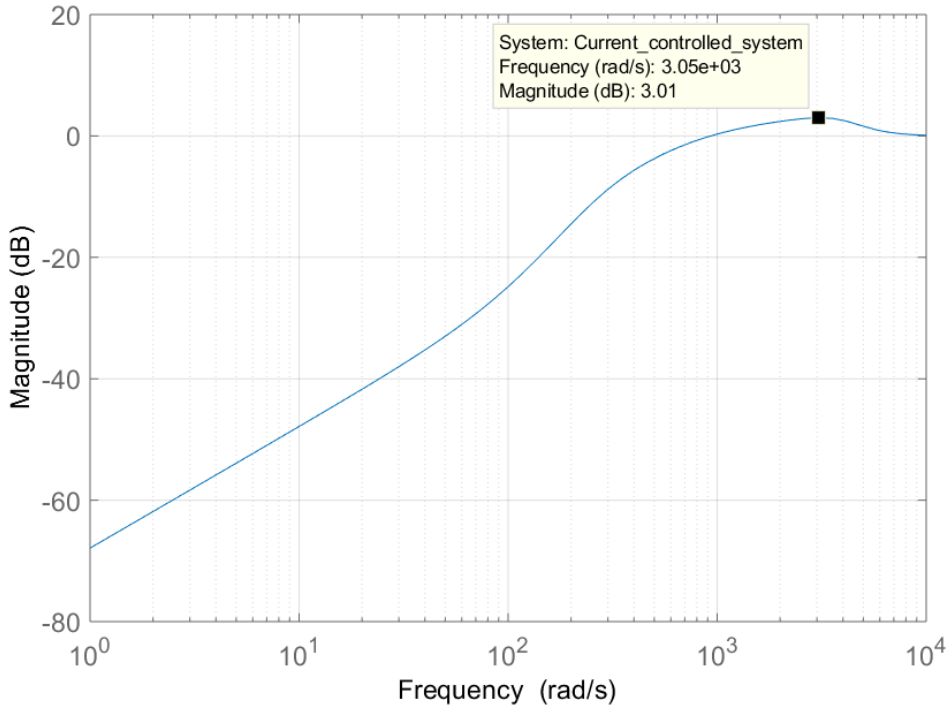

Figure 3.10 – Bode plot of sensitivity function

Peak sensitivity is 1.45 dB, which corresponds to the standards for levitated systems [11] ($10^{\frac{3.01}{20}} = 1.41 < 3$).

Closed loop poles as a combined action of current control and outer position control loops are shown in Figure 3.11.

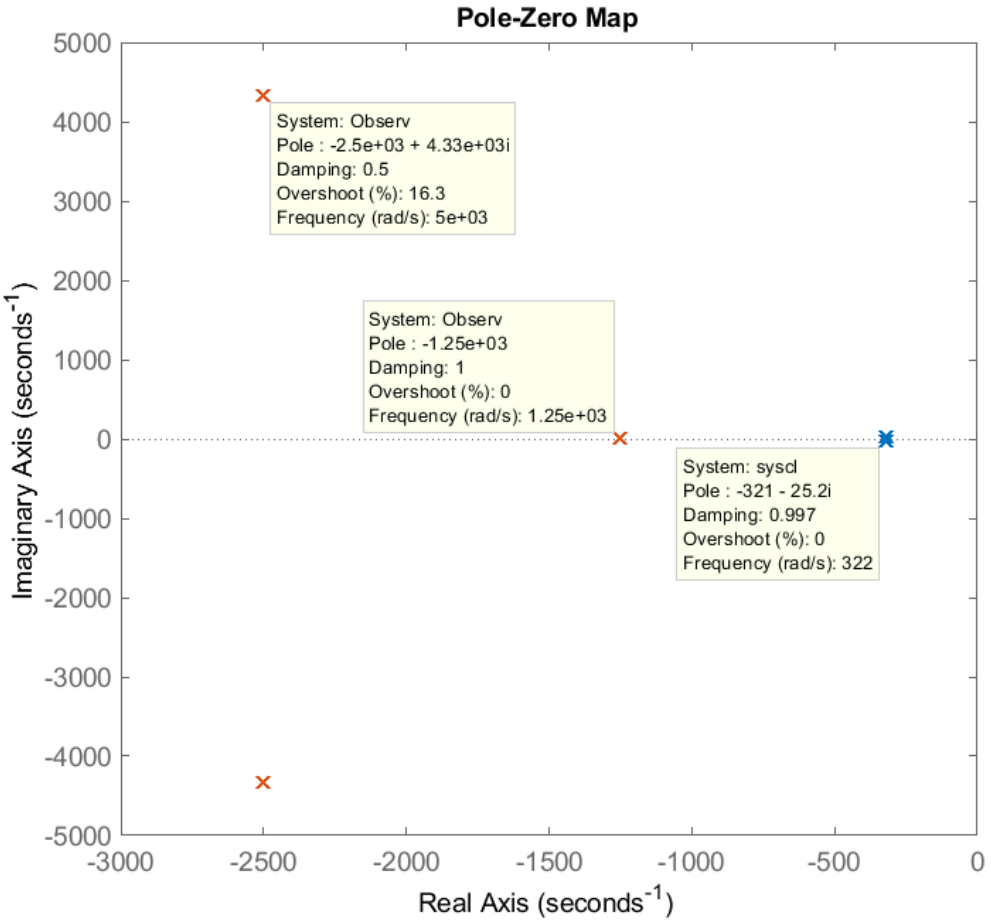

Figure 3.11 – Closed loop poles as a combined action of current control and outer position control loops

As a result of simulation, time responses of reference signal and position, voltages and currents in the electromagnets were obtained.

The control signal is applied at 0.015 second and canceled at 0.15 second, the disturbance equal to 10% of the maximum load applied at 0.25 second and removed at 0.35 second. Rotor position sensor noise is not applied. Time responses of reference signal with position and current acting in lower electromagnet during step reference and step disturbance are shown in Figure 3.12.

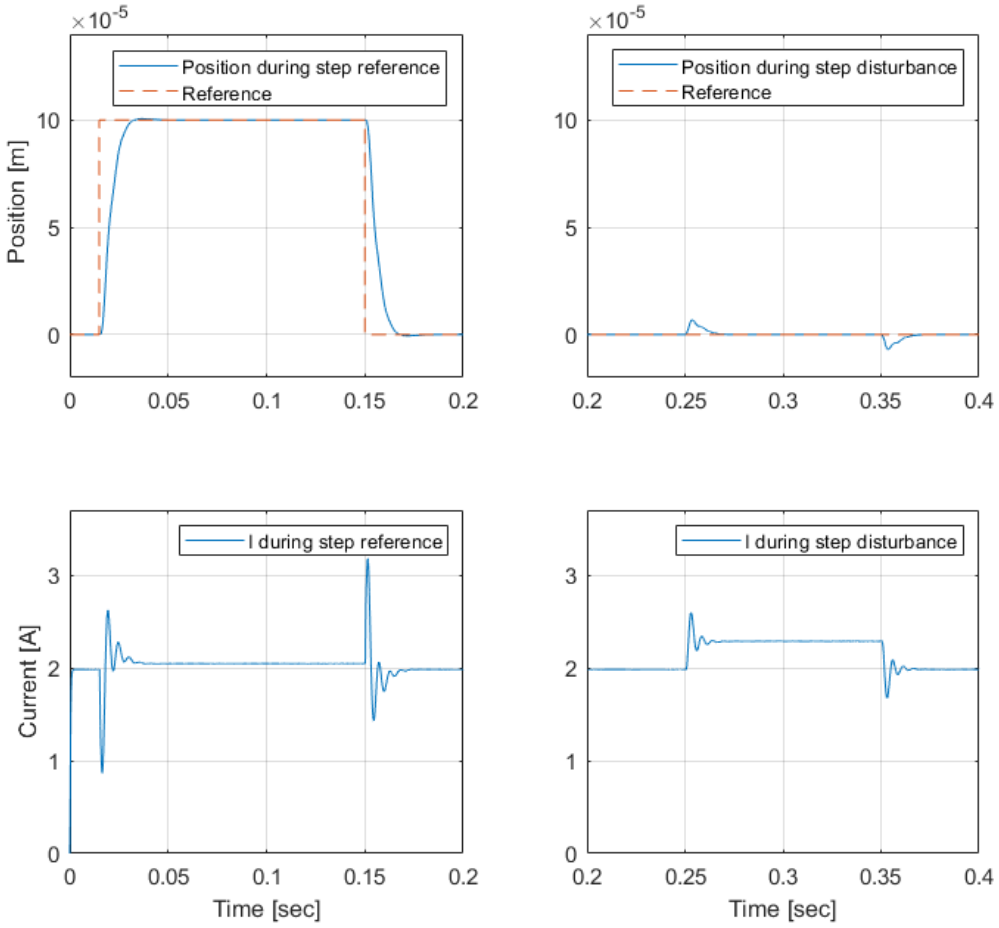

Figure 3.12 – Position and current: during step reference and step disturbance

As a result, we can conclude that system is tuned so, that it has a good position time response for step reference as well as for step disturbance.

On the other hand, system has quite large current oscillations in the electromagnet while responding to step reference and step disturbance.

4 Flux controlled system and DFC

4.1 Flux control

More advanced control principles are flux control and DFC that have same structure for outer position control loop. Main difference with current control system is that current and position stiffnesses are not used, this fact, as expected, allows to achieve better dynamics.

Flux controlled system has the same structure with current controlled but control signal, in this case, is flux instead of current. Flux is estimated using measured currents. Structure of outer position control loop can be seen in Figure 3.1 and flux control system is shown in Figure 4.1.

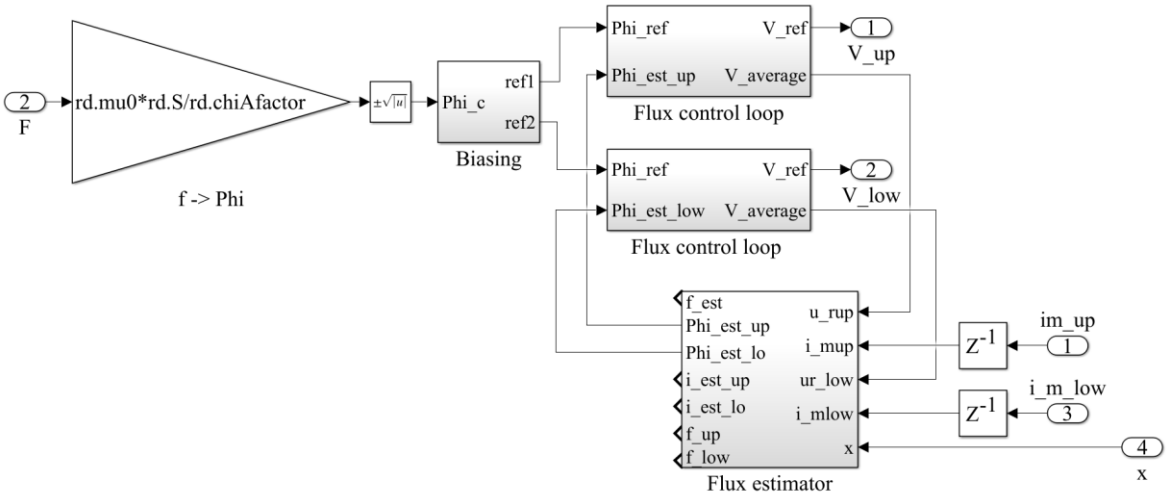

Figure 4.1 Flux control system with flux estimator

Outer position controller provides the reference force signal, f_r, to the inner flux controllers. The reference force is constructed from the bias force, f_0, and the control force signal, f_c, such as $f_r = f_0 \pm f_c$.

The proportional current feedback is replaced with the flux feedback control $u_r = k_\Phi \left(\Phi_r - \Phi_m \right)$, where the measured flux, Φ_m, can be replaced by the esti-

mated value, Φ_{es}. The feedback gain, K_Φ, replaces the current feedback gain, K_c. Neglecting the coil resistance and assuming no saturation and no PWM or measurement delays, the closed inner-loop flux control dynamics, G_{cl}, can be approximated by:

$$G_{cl} = \frac{\Phi_m}{\Phi_r} \approx \frac{K_\Phi}{Ns + K_\Phi}. \tag{4.1}$$

Analogically to the current control, we obtain the maximum bandwidth of the inner flux control (approximated as a first-order system) with respect to the flux rise time from 10% to 90% of the maximum flux value when using the maximum voltage, u_{dc}:

$$\omega_{bw} = \frac{\ln(9) u_{dc}}{0.8 N B_{sat} S_{air}}. \tag{4.2}$$

Equation (4.7) results in a bandwidth that is approximately equal to 1900 Hz for the design value of the saturation magnetic flux density. However, with the inner flux loop, the major concerns are the maximum allowable current in the windings and the resulting saturation of the force control signal. The effects of the magnetic saturation can be taken into account in the flux observer. When rewriting (4.7) in terms of the maximum allowable current and the nominal inductance, we obtain the same maximum bandwidth estimate as for the inner current control loop:

$$\omega_{bw,\ max} = \frac{\ln(9) u_{dc}}{0.8 L i_{max}} \approx 2150 \cdot 2\pi. \tag{4.3}$$

For this comparison, the inner-loop controller bandwidth is selected to have the same bandwidth as in current-controlled method $\omega_{bw} = 880$ Hz [12].

Analogically to the current controlled system, flux feedback gain, K_Φ, can be found in the following way:

$$K_\Phi < \frac{\ln(9) N u_{dc}}{0.8 L i_{max}} = \frac{N}{L} K_c = 564323. \tag{4.4}$$

Force estimator is considered in upcoming subchapter.

4.2 Theory about DTC and DFC

Inherently unstable system should be stabilized, classical current control can be used for this purpose as it is shown above. For more demanding applications, a more sophisticated control system is needed that monitors the electromagnetic state of the machine to more accurately manage force. Consider DTC that is mostly used in electric drives to control AC-motors.

DTC is simple, in principle, requiring only two space vector Equations for control – the voltage integral, which gives an estimate of stator flux linkage, and the torque (or force) Equation.

DTC utilize analytical space-vector models to accurately predict and then control motor or generator status. A DTC controller measures motor currents and calculates voltages and can accurately estimate machine state and control torque in real time. A DTC can increase the force production of an electric machine from zero to its rated value in a few milliseconds. This is especially important for servo drives. Because DTC also improves drive properties in general, it is widely implemented. DTC is seen in both the most demanding and less demanding applications.

In 1984, Manfred Depenbrock from Germany introduced his Direkt Selbstregelung or direct self-control (DSC, 1985). That same year, Isao Takahashi and Toshihiko Noguchi (1986) from Japan introduced a method based directly on Faraday's induction law. In their method, stator flux linkage was estimated by integrating the stator voltage vector:

$$\Psi_{\mathrm{s,est}} = \int \left(u_s - R_{\mathrm{s}} i_{\mathrm{s}} \right) dt \,, \tag{4.5}$$

From the control engineering perspective, the motor current in DTC is an output variable of the system, not an input variable. DFC works in opposite way

with current control, where currents are controlled to regulate flux and force. Flux linkage can be regulated directly by controlling the switches of the inverter.

Applying the appropriate voltage vector in DTC gives possibility to control of the magnitude of stator flux vector and the electromagnetic torque by means of stator flux vector position.

Depending on converter type, there are a different number of different length vectors available for use. In a two-level converter, there are six different active voltage vectors.

In DFC estimated value of acting force is defined by integration of voltage. Estimated currents are used to stabilize the voltage integral same as it is implemented in DTC. Two voltage vectors are used 150 and -150V and so-called zero vector.

In DTC, the voltage model $\Psi_{s,est} = \int (u_s - R_s i_s) dt$, is calculated frequently. For instance, in ABB's classical DTC converters, the computation of the voltage model is repeated every 25 µs. Drifting of the motor flux linkage vector away from the origin because of errors in the voltage model occurs in tens of milliseconds. Therefore, the eccentricity of the flux linkage calculated by the voltage model must be corrected about every millisecond.

In electric current model correction, stator flux linkage integrated from the voltage Ψ_{su} is corrected by an error vector $\Delta\Psi_s$. The current model is the vector equivalent circuit of the electric machine including resistances and inductances.

The error vector is constructed as a difference of the stator flux linkage vector integrated from the voltage (subscript u) and the stator flux linkage vector calculated by the current model (subscript i).

$$\Delta \Psi_s = \Psi_{si} - \Psi_{su} . \tag{4.6}$$

The flux linkage difference of (4.6), suitably weighted, is used to correct the stator flux linkage for instance at every 100th microsecond. During a fast transient, the DTC gives more weight to corrections coming from the voltage model and less weight to corrections suggested by the electric current model. As the transient stabilizes, more and more weight is transferred to the electric current model to keep the motor stator flux linkage vector from drifting into an eccentric orbit [14].

DFC utilize similar principle with some differences, implementation is shown in the following paragraphs.

4.3 DFC

Novel developed control principle is DFC. Structure of outer position control loop is same with current controlled system and can be found in Figure 3.1. The developed position controller as well as for all systems is implemented based on LQG. Electromagnet model used in this section is also nonlinear.

Flux controlled and DFC systems have absolutely the same tuned controller and flux estimator. Controller is tuned in the following way.

$$R = 0.1\left[\frac{1}{f_{\max}{}^2}\right]; \tag{4.7}$$

$$Q = 0.1\begin{pmatrix} \frac{1}{(100x_{\max})^2} & 0 \\ 0 & \frac{1}{(20000V_{\max})^2} \end{pmatrix}. \tag{4.8}$$

Disturbance observer is tuned in the following way.

$\omega_n = 4000\,rad/s$;

$\zeta = 0.5$;

$\alpha = 0.5$.

Estimator gain is obtained with natural frequency:

$\omega_{n2} = 4000\,rad/s$.

Full model contains a part that is fully discretized and loaded into the programmable logic controller. Also, a full model contains a plant model. The model block is shown in Figure 4.2.

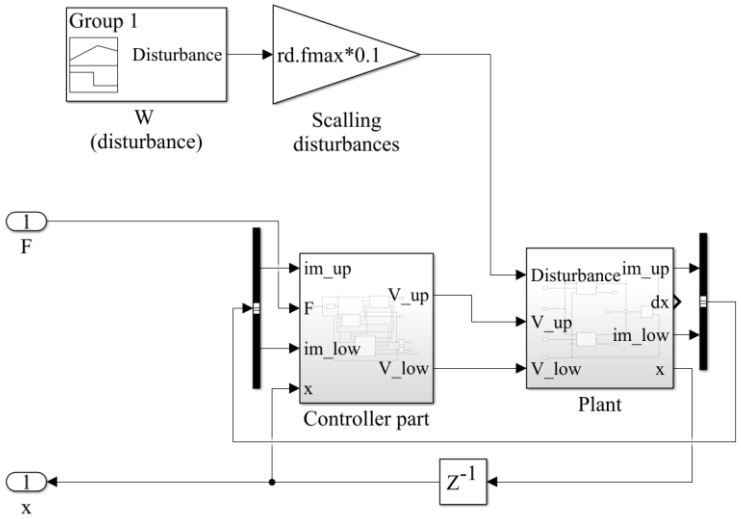

Figure 4.2 – Control system model block

Control system of DFC includes force biasing, modulators for each electromagnet and flux estimator as shown in Figure 4.3.

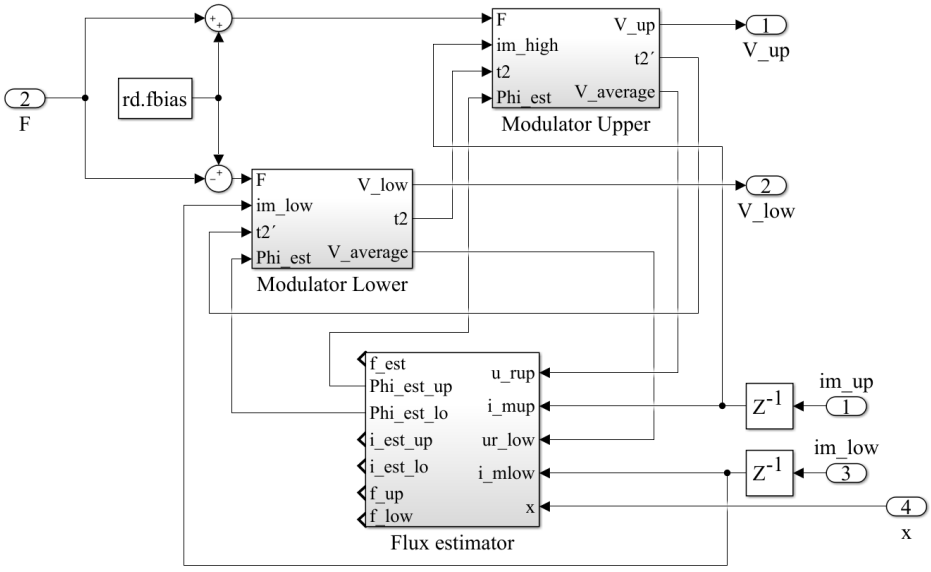

Figure 4.3 – Control system of DFC consisting of force modulators and flux estimator

Required force value is an input to the system provided by the outer position controller. Reference signal is shifted by the value of biasing force for fluctuations elimination in the equilibrium position.

Flux estimator calculates fluxes acting in each electromagnet by measured currents. Delay of current sensors is assumed to be 10μs. Values of these fluxes are used as feedback and subtracted from the desired flux signal.

4.4 Modulator

In DFC it is possible to regulate force directly by controlling the switches of the inverter, so force is fitted as an input to modulator then it is converted to switching duty ratio, and then value of the necessary instant voltage value is provided as an output.

Part intended for recording in the PLC comprises a modulator for each electromagnet.

The reference force can be changed to the reference flux:

$$\Phi_{\mathrm{r}} = \sqrt{f_{\mathrm{r}} \frac{\mu_0 S_{\mathrm{air}}}{cos\chi}} \,. \tag{4.9}$$

Desired flux signal may be converted into on-switching transistor duration at the exact sampling time that is the duration of PWM period according to the following Equation:

$$\Phi = \frac{1}{N} \int \left(u - Ri \right) dt \,. \tag{4.10}$$

Force modulator is shown in Figure 4.4.

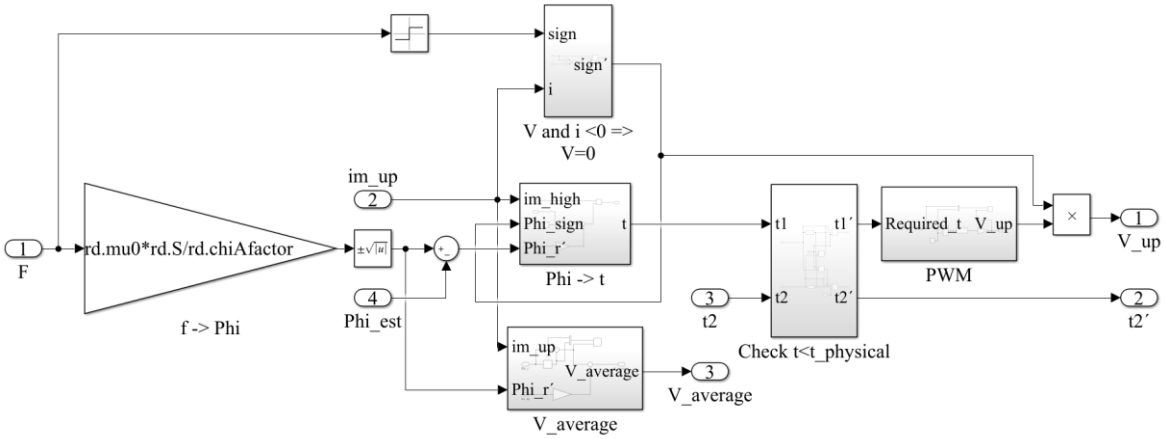

Figure 4.4 – Force modulator, choosing on-switching transistor duration and providing necessary instant voltage value

Instant voltage value is fitted directly to the electromagnet. On the other hand, estimator also requires voltage for computing estimated flux. The fastest physically possible switching time of transistors is assumed to be 4μs but sampling rate of estimator is lower due to delay of current measurement sensors. In this case to avoid estimator picks-up wrong voltage values average voltage in electromagnet is computed according to the following Equation:

$$u = Ri + \frac{d\Psi}{dt}. \tag{4.11}$$

Conversion of desired flux signal to on-switching transistor duration in accordance with Equation (4.10) is shown in Figure 4.5.

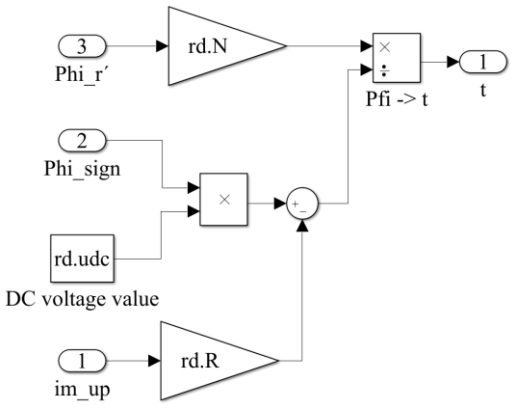

Figure 4.5 – Conversion from reference flux value to on-switching transistor duration

Depending on the desired direction of the force voltage of the same sign is used.

Desired on-switching transistor duration is checked in block «Check t <t_physical», it can not be smaller than a time corresponding to the maximum physically possible switching frequency.

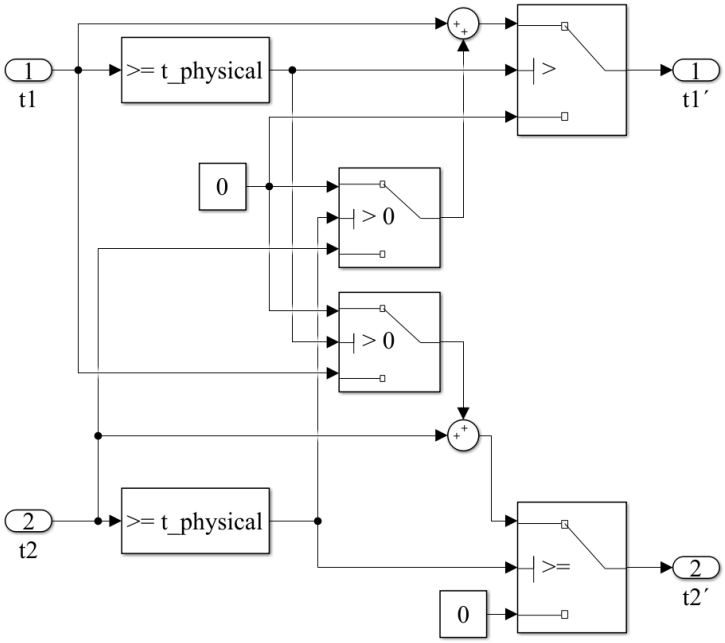

Figure 4.6 – Block that prevent switches faster than physically possible

Then the signal is modeled in «PWM» block and, depending on the required force sign, 3 voltage levels are generated: -150V, 0, 150V. Instant voltage values are applied to the electromagnet.

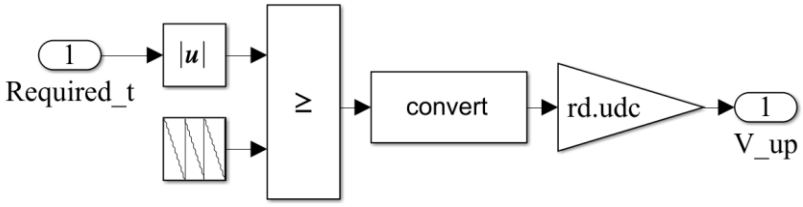

Figure 4.7 – PWM implementation

Required switching time value is compared with triangular signal as shown in Figure 4.8.

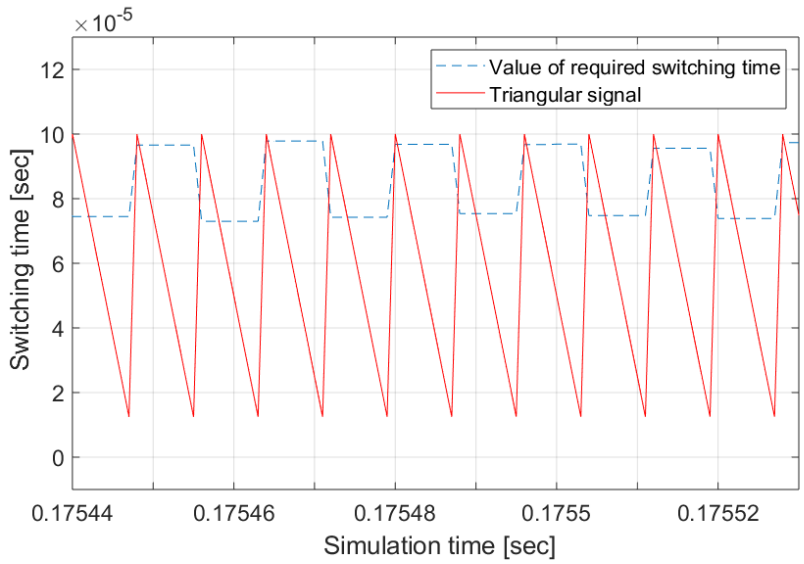

Figure 4.8 – PWM as a comparison of required switching time with triangular signal

Required switching time is a positive value so positive triangular signal is used. To take force direction into account, voltage value obtained from PWM block is multiplied with sign of required force. Resulting modulated voltage and induced current during step disturbance is shown in Figure 4.9.

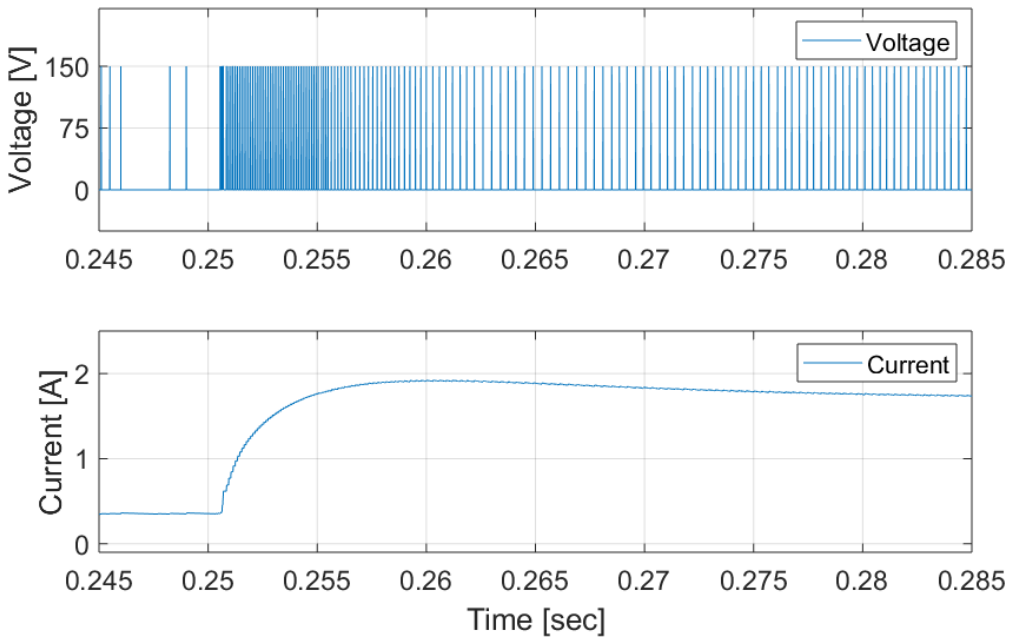

Figure 4.9 – Modulated voltage as a result of PWM and current induced during step disturbance

Negative flux, so negative current as well, do not produce necessary force because according to (2.16), the force has a quadratic dependence on the flux. To avoid negative currents block «Vand i <0 => V = 0» is built. If current in electromagnet becomes negative the zero voltage is supplied.

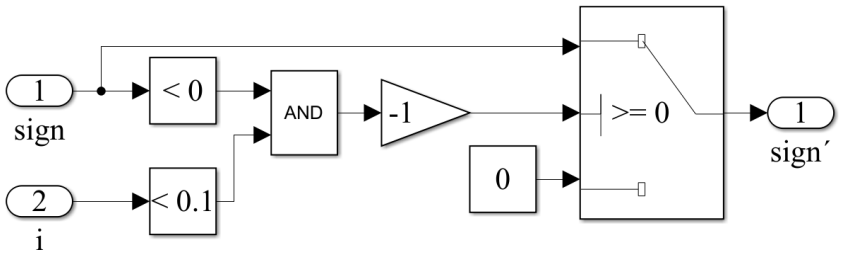

Figure 4.10 – Block that avoid negative currents

Flux estimator is considered in the next subchapter.

4.5 Flux estimator

DFC does not require a flux measurement, flux and forces acting in electromagnet are computed with flux estimator using measured currents.

When not measured, the fluxes can be calculated by integrating the applied voltages, u_1 and u_2, in the electromagnets:

$$\Phi_1 = \frac{1}{N}\int\left(u_1 - Ri_1\right)dt; \tag{4.12}$$

$$\Phi_2 = \frac{1}{N}\int\left(u_2 - Ri_2\right)dt. \tag{4.13}$$

Where applied voltages, u_1 and u_2, are replaced by the corresponding reference values. The estimated flux, Φ_{es}, and current, i_{es}, are computed by using the estimator:

$$\frac{\mathrm{d}\Phi_{es}}{dt} = \frac{1}{N}\left(u_r - Ri_{es}\right) - L_{ob}\left(i_{es} - i\right); \tag{4.14}$$

$$i_{\mathrm{es}} = \Phi_{\mathrm{es}} \frac{l}{N S_{\mathrm{air}} \mu_0} + \frac{l_{\mathrm{Fe}}}{N} H_{\mathrm{Fe}}\left(B_{\mathrm{es}}\right), \tag{4.15}$$

where $H_{\mathrm{Fe}}(B_{\mathrm{es}})$ is implemented as a look-up table-based magnetic saturation model for the iron of the electromagnets. The estimated flux density $B_{\mathrm{es}} = \frac{\Phi_{\mathrm{es}}}{S_{\mathrm{air}}}$, l and l_{Fe} are the flux paths in the air and in the iron of the AMBs. In this work, the observer feedback gain, L_{ob}, is computed when using the linearized model and placing the closed-loop pole, so that its natural frequency and damping ratio are 1760 Hz and one, respectively. The current feedback in the flux estimator corrects the integration of the applied voltages. The described flux estimator works well in the case of laminated radial AMBs. For the cases where high eddy currents and stray fluxes are expected, it is possible to include these effects in the observer when considering the axial bearing [12].

Estimator discretized according to bilinear (Tustin) approximation method, Laplace operator s of integrator is replaced in following way:

$$s = \frac{2}{T} \frac{z-1}{z+1}, \tag{4.16}$$

where T is sampling time.

The estimator is modeled by the Equations (4.14) and (4.15) and is shown in Figure 4.11.

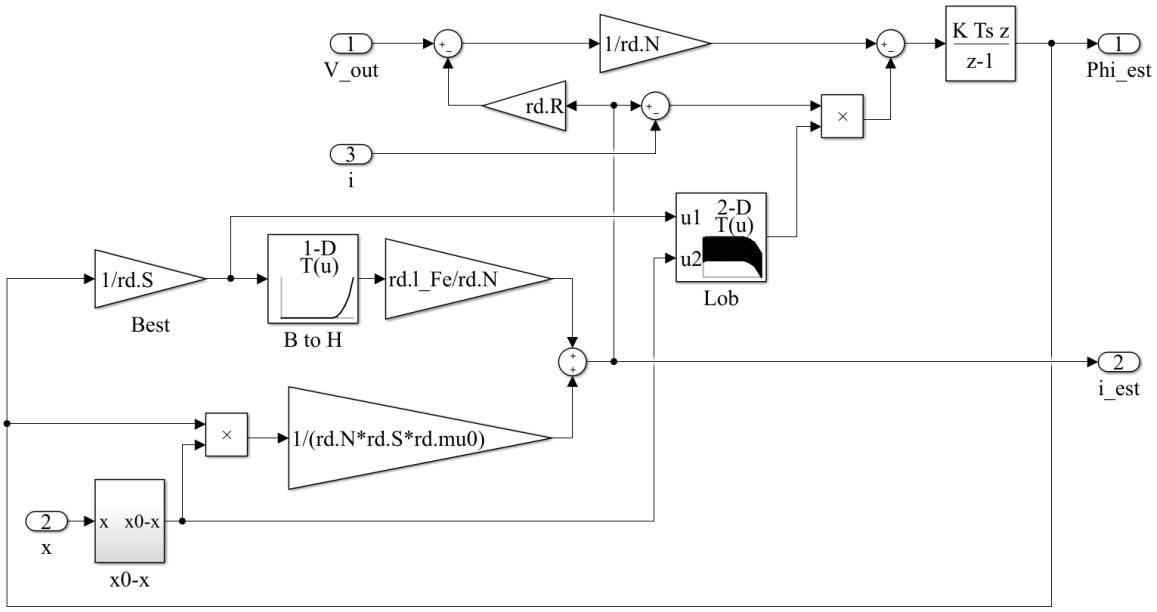

Figure 4.11 –Flux estimator, providing estimated flux and estimated current in the electromagnet

L_{ob} is precalculated 2 dimensional look up table [18x41] with 2 inputs that are μ_r (so L_{ob} depends on flux) and displacement. 18 points for μ_r are obtained from $B(H)$ curve for steel number "Sura NO 20", 41 points for displacement are chosen taking into account length of airgap and possible displacement. Thus estimator gain is a function that depends on the flux and position.

Estimator is built as a state-space model. Estimator gain is obtained using pole placement. Wherein ω_n is varied to obtain desired poles. Function L = *acker ()* is used to obtain the estimator gain.

Block that takes into account the influence of displacement of the rotor is shown in Figure 4.12.

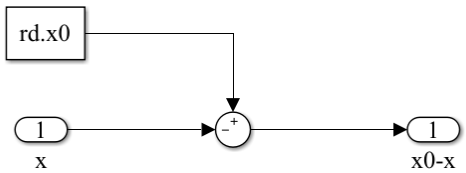

Figure 4.12 – Block taking into account the displacement of the rotor relative to the upper electromagnet

Displacement of the second rotor electromagnet is taken into account in similar way, but with an opposite sign.

According to Equation (4.9) flux estimator is modeled so that it provides estimated force for each of the electromagnet and the resulting estimated force action of both electromagnets. This block is shown in Figure 4.13.

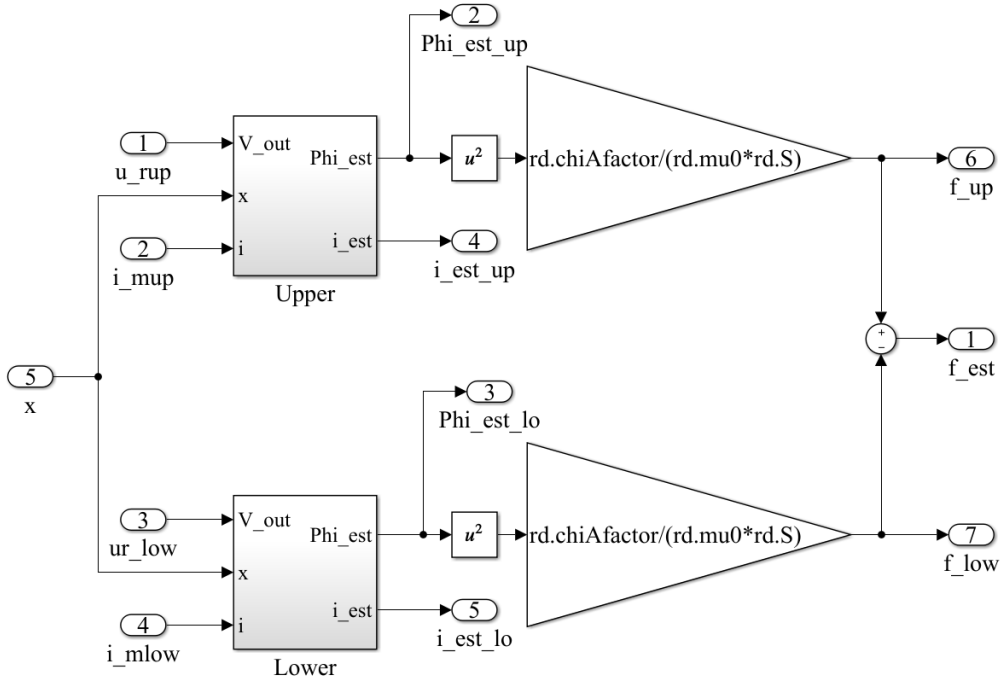

Figure 4.13 – Flux estimator block, providing values of estimated fluxes and force as a result of acting both electromagnets

As a result of the simulation flux and estimated flux of the lower electromagnet are compared. Graphs are shown in Figure 4.14.

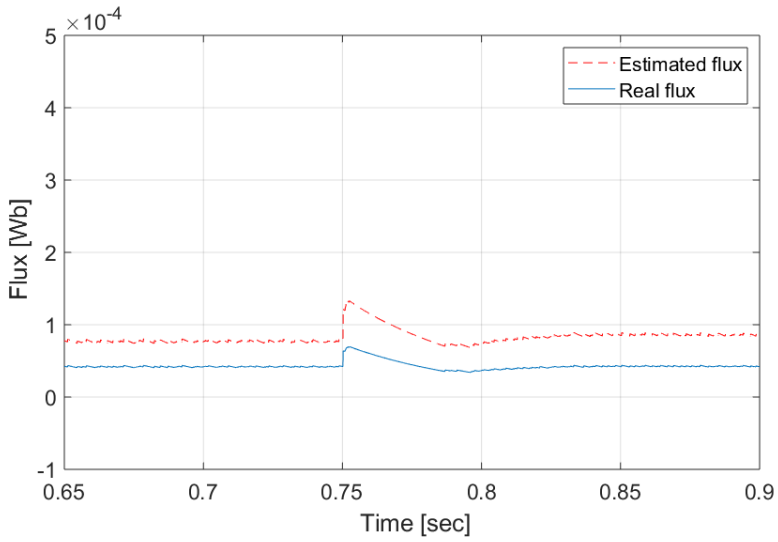

Figure 4.14 – Accuracy of estimated flux relative to the real one

It can be seen, that estimated flux follows the real one with some acceptable uncertainty.

4.6 Simulation results

Frequency response to determine the sensitivity function to disturbance and noise is shown in Figure 4.15.

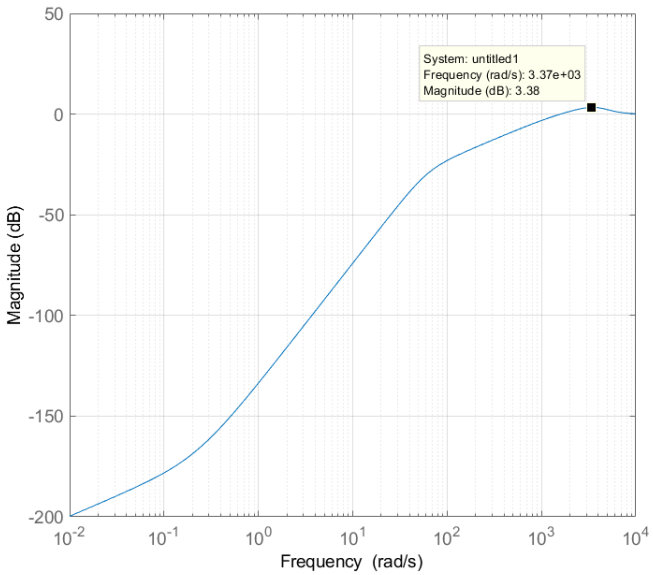

Figure 4.15 – Closed loop poles of flux controlled and DFC systems

Same controller is used for both flux controlled and DFC systems. Closed loop poles are shown in Figure 4.16.

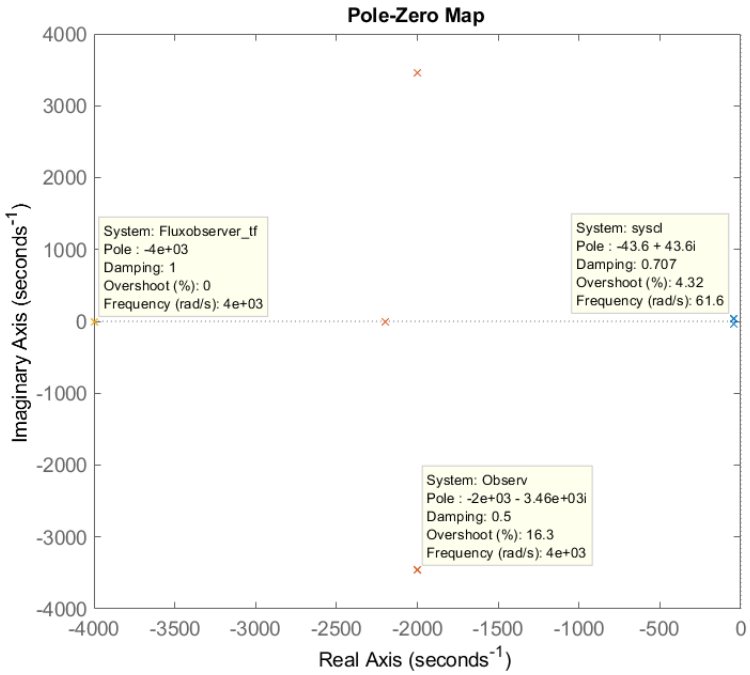

Figure 4.16 – Closed loop poles of flux controlled and DFC systems

It is relevant to compare DFC and flux controlled systems and it is of particular interest. So position time responses for both systems are obtained. Disturbance value, as well as for systems with current control, is 10% of maximum allowable load.

The reference signal is applied at 0.015 second and canceled at 0.75 second, the disturbance is applied at 0.25 second and removed at 0.5 second. Position sensor measurement noise was not taken into account.

For proper comparisons the same scaling was used and the same control signals and the disturbances were applied.

Reference step response and disturbance step response for DFC and flux controlled systems are shown in Figures 4.17 and 4.18 relatively.

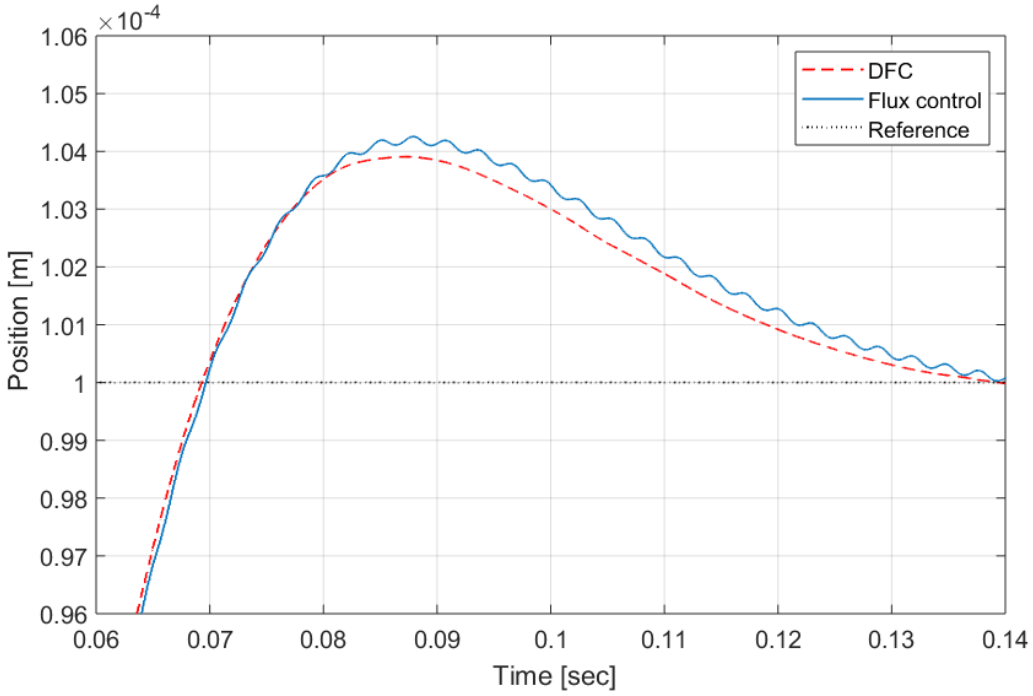

Figure 4.17 – Reference step response for DFC and flux controlled systems

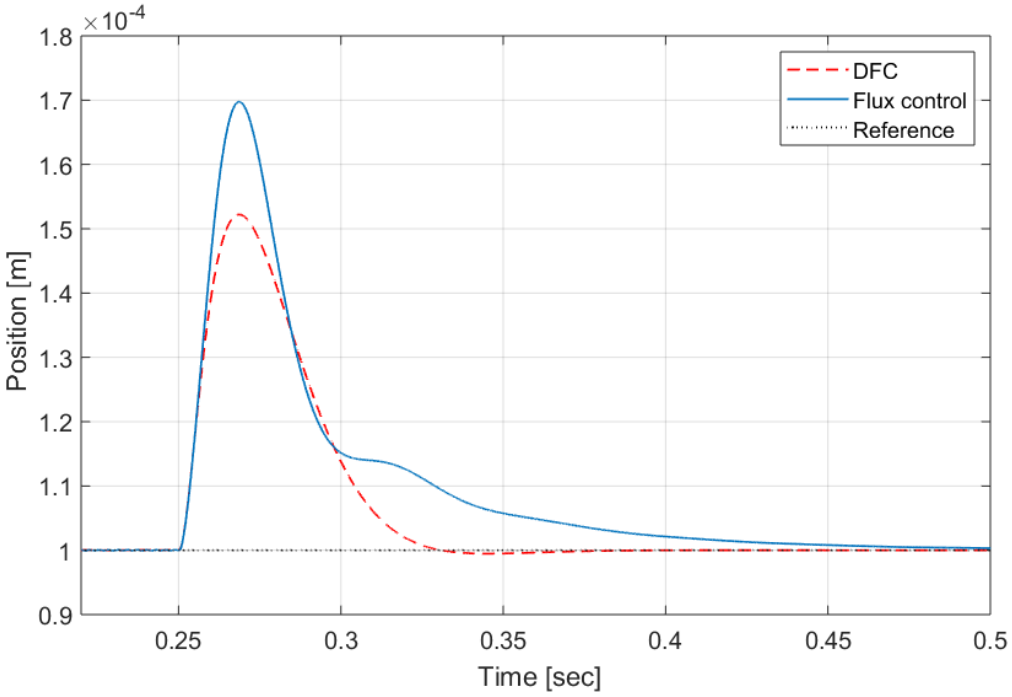

Figure 4.18 – Disturbance step response for DFC and Flux controlled systems

Times scale is different from the one used for current controlled system because flux controlled and DFC systems happened to be slower.

It can be seen that for two observable systems with the absolutely same controller reference step response of DFC is slightly faster and smoother, while flux controlled system has some oscillations. Furthermore, disturbance response of DFC is much better than disturbance response of flux controlled system, in particular, overshoot is lower and settling time is quite smaller.

For monitoring the plant electromagnetic behavior currents of lower electromagnet for the same control conditions are compared for both systems in Figure 4.19.

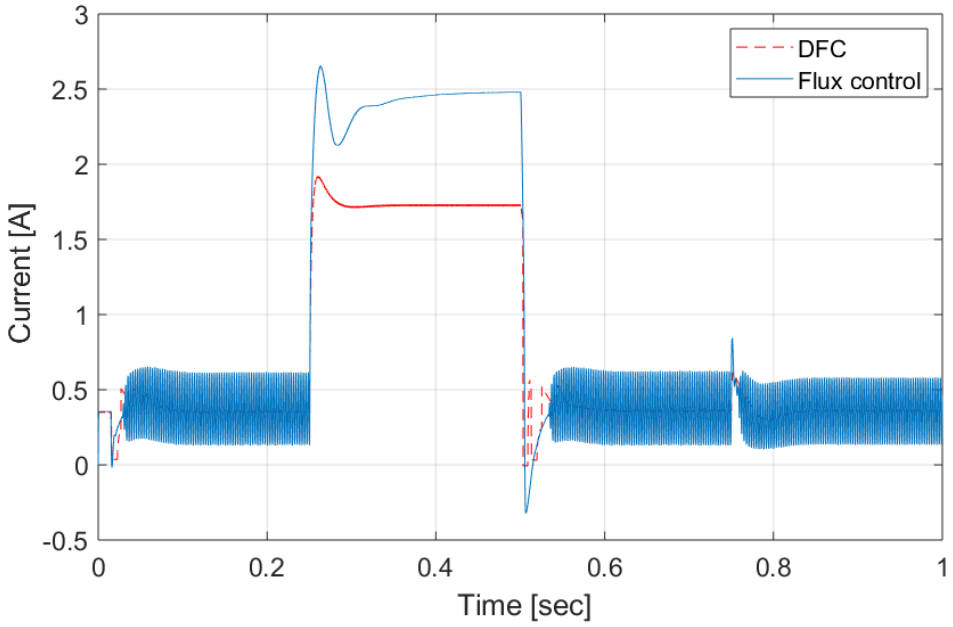

Figure 4.19 – Current for DFC and flux controlled systems

It can be seen that DFC has lower current under load and quite smooth behavior without load, while flux controlled system has large oscillations working without load.

We can conclude that DFC system with the same tuned controller and the same plant model acts better, than flux controlled system. Namely, position reference time response is slightly faster, position disturbance time response is much faster and has no oscillations, currents are smaller and do not have oscillations, while working without load.

CONCLUSION

In this work ways to build and configure a linear quadratic regulators were studied, as well as ways to create and tune control systems for active magnetic bearings.

As a result, three systems are constructed: the current controlled, flux controlled and DFC. Dynamics of systems are compared using position and disturbance time responses, current and voltage curves.

Flux controlled system has a better performance in reaction to the disturbance, and ripple currents are much smaller than in the current control system.

Despite of better dynamics of DFC on this step, one option to increase dynamic even further is to build a predictive controller. The main idea of such a control method is the fact that it is possible to determine necessary voltage several steps earlier. It will require modification of existing modulators.

Another way is to use control force command without flux feedback. This means there is a possibility to avoid using estimator that slows down the system. Preliminary studies showed that it is possible, moreover, system has better dynamics. But further research is still required to present exact results.

Future work is going to consist of the following steps: comparison of controllers for flexible rotor models, experimental results validation.

REFERENCES

1. Boerdijk, A. H. Technical aspects of levitation // Philips Res. Rep. – 11. – 1965. – P. 45-56.

2. Geary, P. J. Magnetic and electric suspensions // BSIRA. – R314. – London. – 1964. – P. 162.

3. Braunbek, W. Freischwebende Korper im elektrischen und magnetischen Feld // Z. fur Phisic. – 112. – 1939. – S. 753-765.

4. Lyman, J. United States Patent No. 3243238. Magnetic suspension. United States Patent Office, 1966.

5. Фомин, А. А. Бесконечный цилиндр в поле коаксиальной системы витков.

6. Фомин, А. А. Исследование цилиндрического индуктора с экспоненциальным полем //Магн. гидродинамика. 1966. № 3. С.92-100.

7. Фомин, А. А. Расчет симметричного индуктора с мультипольным полем // Магн. гидродинамика. 1966. № 2. С. 124-129.

8. Milyutin, A.Y, Temnikov, E.A, Gottfried, P.A Application of magnetic systems (hangers) in the design of windmills// Scientific forum: Technical and physical and mathematical sciences: coll. Art. on the materials of the X. scientific-practical. Conf. - No. 9 (10). - M., Ed. "ICNO", 2017. - P. 130-139.

9. Zhuravlev, Y. N. Active magnetic bearings: Theory, calculation, application // SPb .: Politechnica, 2003. - 206 p.

10. Mirlenko, P. Direct force control of AMB-rotor system, Master’s thesis, LUT, Finland, 2017.

11. Design and implementation of FPGA-based LQ control of active magnetic bearings, Rafal Piotr Jastrzebski.IEEE Trans. Magn. 2007, 161, 1056-4491.

12. Cascaded Position-Flux Controller for an AMB System Operating at Zero Bias, Rafal P. Jastrzebski, Alexander Smirnov, Arkadiusz Mystkowski and Olli Pyrhönen.IEEE Trans. Magn. 2014, 15, 1996-1073.
13. Schneider, D.M., Control of processes with time delays, IEEE Transactions on Industry Applications, Vol. 24, No. 2, March/April, 1988, pp. 186-191.
14. J. Pyrhönen, V. Hrabovcova, S. Semken, Electrical Machine Drives Control: An Introduction, Lappeenranta University of Technology, Electrical Engineering department, Finland 2016.
15. Marc S. Petit, Robert D. Lorenz, Caleb W. Secrest, Brent S. Gagas Dual Control Drives for Increased Capability, EPE'18 ECCE Europe, 2018.

APPENDICES

Appendix 1. The parameters of the current controlled system

Current controlled system parameters are shown in the program code.

```
% Sample time
simp.Ts = 100e-6;
% Rotor mass
rd.m = 18.1273; % kg
% Number of coil turns
rd.N = 65;
% Nominal inductance
rd.L = 0.0016; % H
% Nominal resistance
rd.R = 1.69;
% Nominal airgap
rd.x0 = 0.001; % m
% Mechanical airgap
rd.xmax = 0.0005;
% Biasing current
rd.ibias = 8; % A
rd.imax = 20; % A
% DC link voltage
rd.udc = 150; % V
% Cross section area of an electromagnet
rd.S = 6.10e-4;
% Position stiffness
rd.kx = 1.8518 * 10e5;
% Current stiffness
rd.ki = 23.1469;
% Permiability of vacuum
rd.mu0 = 4 * pi * 10 ^ -7;
```

Appendix 2. Parameters of the flux controlled system

Parameters of the flux controlled system are shown in the program code.

```
% Min switching time
t_physical = 4e-6;
% Sample time
simp.Ts = 100e-6;
% Rotor mass
rd.m = 18.1273; % kg
% Number of coil turns
rd.N = 65;
% Nominal inductance
rd.L = 0.0016; % H
% Nominal resistance
rd.R = 1.69;
% Nominal airgap
rd.x0 = 0.001; % m
% The flux path in the iron
rd.l_Fe = 0.108; % m
% Mechanical airgap
rd.xmax = 0.0005;
% Biasing current
rd.ibias = 8; % A
rd.imax = 20; % A
% DC link voltage
rd.udc = 150; % V
% Cross section area of an electromagnet
rd.S = 6.10e-4;
% Permiability of vacuum
rd.mu0 = 4 * pi * 10 ^ -7;
```

Appendix 3. Rigid rotor matrices deriving

Process of rigid rotor matrices deriving is shown in code.

```
El.zm = 0.49175; % center of mass
El.m = 19.26221; % mass
El.Ix = 1124268289.67e-9; % inertia x
El.Iy = 1124268289.67e-9; %El.Ix;
El.Iz = 9547357.86e-9;        % inertia z
El.ki = rd.ki % current stiffness
El.kx = rd.kx % position stiffness

% Assuming center of mass between all elements
El.amb.d_A = El.zm - 0.16; % distance between AMB A and center of mass
El.amb.d_B = 0.7625 - El.zm; % distance between AMB B and center of mass
El.sen.d_A = El.zm - 0.095;% distance between sensor A and center of mass
El.sen.d_B = 0.8225 - El.zm;%distance between sensor B and center of mass

% Select modal masses as actual masses and inertias
m.Mm = diag([El.m,El.m,El.Ix,El.Iy]);
m.Gm = [0          0          0          0
        0          0          0          0
        0          0          0          1
        0          0         -1          0]*El.Iz;
m.Km = zeros(4); % No rotor mechanical stifness
m.Dm = zeros(4); % No rotor mechanical damping
Omega = 0; % Assume zero speed
Ki = El.ki*eye(4);
Kx = El.kx*eye(4);
m.Tb = [1           0          0          -El.amb.d_A
        0           1          El.amb.d_A  0
        1           0          0           El.amb.d_B
        0           1         -El.amb.d_B  0];
m.Ts = [1           0          0          -El.sen.d_A
        0           1          El.sen.d_A  0
        1           0          0           El.sen.d_B
        0           1         -El.sen.d_B  0];

rotor.C0b = [m.Tb zeros(4)]; % output at bearings from CofG
rotor.C0s = [m.Ts zeros(4)]; % output at sensors from CofG)

rotor.Asy = [ zeros(4)    eye(4);
             -m.Mm\m.Km  -m.Mm\(m.Dm+Omega*m.Gm)];

% Now m.Tb is our matrix for congruent transformation of stiffness'
rotor.A0 = [ zeros(4)                          eye(4);
            -m.Mm\(m.Km + (m.Tb')*Kx*m.Tb) -m.Mm\(m.Dm+Omega*m.Gm)];
rotor.B0 = [zeros(4); m.Mm\(m.Tb')*Ki];
rotor.C0 = rotor.C0s;
rotor.D0 = zeros(4);
rotor.m = m;
 % same as:
Keyem = m.Tb';
Bamb = [zeros(4); m.Mm\Keyem];
rotor.A02 = rotor.Asy + Bamb*Kx*rotor.C0b;
rotor.B02 = Bamb*Ki;
```